Dynamics of Elevated Vortices

ALAN SHAPIRO AND PAUL MARKOWSKI

School of Meteorology, University of Oklahoma, Norman, Oklahoma

(Manuscript received 26 August 1997, in final form 8 June 1998)

ABSTRACT

Theoretical hydrodynamic models for the behavior of vortices with axially varying rotation rates are presented. The flows are inviscid, axisymmetric, and incompressible. Two flow classes are considered: (i) radially unbounded solid body–type vortices and (ii) vortex cores of finite radius embedded within radially decaying vortex profiles.

For radially unbounded solid body–type vortices with axially varying rotation rates, the von Kármán–Bödewadt similarity principle is applicable and leads to exact nonlinear solutions of the Euler equations. A vortex overlying nonrotating fluid, a vortex overlying a vortex of different strength, and more generally, a vortex with N horizontal layers of different rotation rate are considered. These vortices cannot exist in a steady state because continuity of pressure across the horizontal interface between the vortex layers demands that a secondary (meridional) circulation be generated. These similarity solutions are characterized by radial and azimuthal velocity fields that increase with radius and a vertical velocity field that is independent of radius. These solutions describe nonlinear interactions between the vortex circulations and the vortex-induced secondary circulations, and may play a role in the dynamics of the interior regions of broad mesoscale vortices. Decaying, amplifying, and oscillatory solutions are found for different vertical boundary conditions and axial distributions of vorticity. The oscillatory solutions are characterized by pulsations of vortex strength in lower and upper levels associated with periodic reversals in the sense of the secondary circulation. These solutions provide simple illustrations of the ''vortex valve effect,'' sometimes used to explain cyclic changes in updraft and rotation strength in tornadic storms.

A linear analysis of the Euler equations is used to describe the short-time behavior of an elevated vortex of finite radius embedded within a radially decaying vortex profile (i.e., elevated Rankine-type vortices). The linear solution describes the formation of a central updraft (as in the similarity solution) and an annular downdraft ringing the periphery of the vortex core (not accounted for in the similarity solution). Downdraft strength is sensitive to both the vortex core aspect ratio and outer vortex decay rate, being stronger and narrower for broader vortices and larger decay rates. It is hypothesized that this dynamically induced downdraft may facilitate the transport of mesocyclone vorticity down to low levels in supercell thunderstorms.

1. Introduction

The behavior of axisymmetric hydrodynamic vortices with axially varying rotation rates is investigated. We consider two classes of vortex flows: (i) radially unbounded solid body–type vortices and (ii) vortex cores of finite radius embedded within a radially decaying vortex profile. Both classes include the case of a vortex overlying nonrotating fluid. For the first type of flows, the von Kármán–Bödewadt similarity principle is applicable and leads to new exact solutions of the nonlinear Euler equations. These similarity solutions describe the induction of secondary (meridional) circulations in radially unbounded solid body vortices, and the subsequent feedback of these circulations on the vortex circulations. These solutions provide a description of nonlinear processes that may occur in the interior regions of broad geophysical vortices. Decaying, amplifying, and oscillatory solutions are found for different vertical boundary conditions and axial distributions of vorticity. The oscillatory solutions are characterized by pulsations of vortex strength in lower and upper levels associated with periodic reversals in the sense of the secondary circulation. The oscillatory behavior appears to be a manifestation of the ''vortex valve effect,'' a dynamical mechanism used to explain the ''choking'' of updrafts in vortex chambers and the morphological changes observed in some tornadic storms (Lemon et al. 1975; Davies-Jones 1986).

Our study of the second class of vortex flows is motivated by a basic question concerning low-level mesocyclogenesis and associated tornadogenesis: in the absence of precipitation and thermodynamic effects, how should an isolated elevated vortex behave? To gain insight into this problem we perform a linear analysis of the Euler equations for an elevated vortex of finite core radius (in the exact solutions described above the solid body rotation extended to infinity—now we consider an inner core in solid body rotation embedded within a

Corresponding author address: Dr. Alan Shapiro, University of Oklahoma, 100 E. Boyd, Room 1310, Norman, OK 73019.
E-mail: ashapiro@ou.edu

radially decaying outer vortex). The analysis, valid for small times, indicates the formation of an annular downdraft on the periphery of the vortex core. The downdraft is stronger and narrower for broader vortex cores and for more rapid radial decay rates in the outer vortex. On the basis of these results we speculate that ''internal'' storm dynamics associated with vertical gradients of vorticity may induce or facilitate downdraft formation on the periphery of elevated mesocyclones (though precipitation and asymmetric effects are obviously important as well). We speculate further that such a dynamically induced downdraft can transport vorticity to lower levels.

To see why elevated vortices cannot exist in a steady state, consider the simplest example of a radially unbounded vortex overlying nonrotating fluid. Continuity of pressure across the horizontal interface separating the upper vortex from the lower nonrotating fluid demands that an inward-directed pressure gradient force be impressed in the nonrotating flow as well as in the rotating flow. As a consequence of this pressure gradient force, a secondary circulation develops such that the nonrotating fluid moves inward and upward (assuming the flow is bounded by a lower impermeable boundary), while the vortex is displaced upward and outward (assuming the flow is bounded either by an upper impermeable boundary or a region of high static stability). Vortex strength subsequently decreases due to the ''squashing'' of vortex lines in the thinning upper layer. If we modify the scenario so that the low-level vorticity is not zero but is smaller than in the upper layer, a secondary circulation should develop as before, but now the low-level vorticity can be stretched and amplified. When the strength of the low-level vortex exceeds that of the upper-level vortex, the secondary circulation should begin to weaken. The evolution of the secondary circulation and its feedback on the vortex circulation through nonlinear processes are the subjects of this investigation.

The difficulty in solving the equations of fluid motion analytically stems from the presence of nonlinear terms associated with fluid inertia. Exact solutions have been obtained only in the special cases for which the nonlinearity could be cast in a tractable form, typically for flows characterized by a few degrees of freedom. The explicit dependence of an exact solution on a few key parameters collapses an infinite number of equivalent numerical simulations into one solution, thereby facilitating the analysis of flow structure and behavior. These rare solutions are prized for their insights into fundamental fluid flows and their utility as test solutions for the validation of numerical flow models (Shapiro 1993).

We now briefly review some of the exact vortex solutions of the Navier–Stokes, Euler, and shallow water equations. Vortex solutions and vortex dynamics in general are surveyed in Greenspan (1968), Lugt (1983), and Saffman (1992).

Exact vortex solutions of the Navier–Stokes equations for viscous incompressible flow include the decaying line vortex (Batchelor 1967), Taylor's decaying vortex grid (Rosenhead 1963), the interaction of a potential vortex with a solid boundary (Serrin 1972; Yih et al. 1982; Paull and Pillow 1985), a vortex in a converging stagnation point flow (Burgers 1948; Rott 1958, 1959), axial flow reversal in a two-celled vortex in stagnation point flow (Sullivan 1959), unsteady multicellular vortices in stagnation point flow (Bellamy-Knights 1970, 1971; Hatton 1975), decaying viscous vortices satisfying the Beltrami condition for alignment of the velocity and vorticity vectors (Shapiro 1993), flow due to an infinite rotating disk (von Kármán 1921), and the closely related solution for the interaction of a solid body vortex with a stationary plate (Bödewadt 1940; Zandbergen and Dijkstra 1987). We also mention Long's well-known viscous vortex (1958, 1961), which complemented his inviscid theory for rotating flow drawn into a sink at the base of a cylinder (Long 1956). However, Long's viscous vortex is not quite a bona fide exact solution of the Navier–Stokes equations since an internal boundary-layer approximation was made. Similarity solutions for steady and unsteady convective atmospheric vortices have been described by Gutman (1957), Kuo (1966, 1967), and Bellamy-Knights and Saci (1983).

These and other exact solutions of the Navier–Stokes equations are sometimes used as proxies for tornadolike vortices (Davies-Jones 1986; Lewellen 1993). For instance, the paradigm of ''vorticity diffusion balancing advection'' embodied by the viscous stagnation point flow vortices of Burgers, Rott, Sullivan, Bellamy-Knights, and others may be relevant to the inner core of tornadoes and other intense vortices. On the other hand, the secondary circulations in these stagnation flow–type vortices are dynamically decoupled from the azimuthal velocity component. This decoupling readily permits an analytic solution to be obtained, but is probably not realistic for most geophysical vortices (including the tornado). We also note that the secondary circulations in these stagnation flow type vortices have a singularity at infinity (a similar singularity also being present in the von Kármán–Bödewadt-type solutions and in the solutions described in our present study). If we restrict attention to the core region, the existence of this singularity may not be troublesome. In contrast, the axial singularity in Serrin's vortex (which acts as a spinning wire) actually drives the flow, and is more offensive than the stagnation flow type singularity for the study of the core region. On the other hand, Serrin's vortex provides one of the few exact solutions of the Navier–Stokes equations in which both the impermeability and no-slip conditions are enforced on a rigid horizontal boundary. The near-surface flow of Serrin's vortex beyond the core region may be a useful analog for the frictional boundary layer in the region of tornadoes beyond the radius of maximum wind. Indeed, the inverse distance velocity scaling characterizing Serrin's vortex (and other, simpler vortices such as the Rankine vortex)

has been observed in real tornadoes (Wurman et al. 1996).

Exact vortex solutions of the Euler equations for inviscid flow include the Rankine vortex (circular patch of constant vorticity), Kirchoff's rotating elliptical vortex patch (Lamb 1945), elliptical vortex patch in a uniform straining field (Moore and Saffman 1971), Hill's (1894) propagating spherical vortex, simple configurations of mutually advecting line vortices (Lamb 1945; Saffman 1992; Aref et al. 1992), inviscid Beltrami flows (Lilly 1983, 1986; Davies-Jones 1985), inviscid sink vortex (Long 1956), and vortex flows through turbomachinery (Bragg and Hawthorne 1950). A class of exact polynomial solutions of the shallow water equations, which includes some vortex solutions, has been studied by Ball (1964), Thacker (1981), Cushman-Roisin (1984, 1987), and Cushman-Roisin et al. (1985), with Cushman-Roisin applying his elliptical vortex solution to oceanic warm-core rings. The exact solutions described in our present study are very closely related to these shallow water solutions.

The organization of this paper is as follows. In section 2 we show how the Euler equations for radially unbounded solid body–vortex-type flows reduce to a simpler form under the von Kármán–Bödewadt similarity principle. In section 3 we set up the problem of an N-layer vortex flow satisfying this similarity principle and characterized by radial and azimuthal velocity fields that are piecewise constant functions of height. The N-layer flow is bounded at the bottom by an impermeable plate, and is either bounded at the top by an impermeable plate or is unbounded vertically. Exact analytic solutions are derived in section 4 for two-layer ($N = 2$) flows. We consider (i) a vortex overlying nonrotating fluid and (ii) a vortex overlying a vortex of different strength. Numerical results for some particular three-layer vortices ($N = 3$) are presented in section 5. In section 6 we turn attention to an elevated vortex core in solid body rotation embedded within a radially decaying outer vortex, a specification that includes the classical (but elevated) Rankine vortex. The presence of the radial length scale greatly complicates the analysis, and we abandon a pursuit of nonlinear solutions in favor of a linear analysis valid for small times. A summary and discussion follow in section 7.

2. Similarity hypothesis and its consequences

The governing equations for inviscid, axisymmetric vortex flows are the Euler equations, expressed in cylindrical polar coordinates (r, ϕ, z) as,

$$\frac{\partial u}{\partial t} + u\frac{\partial u}{\partial r} + w\frac{\partial u}{\partial z} - \frac{v^2}{r} = -\frac{1}{\rho}\frac{\partial p}{\partial r}, \tag{1}$$

$$\frac{\partial v}{\partial t} + u\frac{\partial v}{\partial r} + w\frac{\partial v}{\partial z} + \frac{uv}{r} = 0, \tag{2}$$

$$\frac{\partial w}{\partial t} + u\frac{\partial w}{\partial r} + w\frac{\partial w}{\partial z} = -\frac{1}{\rho}\frac{\partial p}{\partial z}. \tag{3}$$

We also consider the flow to be incompressible,

$$\frac{\partial u}{\partial r} + \frac{u}{r} + \frac{\partial w}{\partial z} = 0. \tag{4}$$

Here u, v, and w are the radial, azimuthal (swirling), and vertical velocity components, respectively, ρ is the (constant) density, and p is the perturbation pressure (deviation of the total pressure from a hydrostatic reference state).

The initial azimuthal velocity profile consists of solid body rotation, $v(r, z, 0) = \Omega(z)r$, with the angular velocity $\Omega(z)$ varying in a prescribed manner along the axis of symmetry. The flow is unbounded in the radial direction and there is a singularity at radial infinity. A secondary circulation is anticipated to develop in the flow, with the azimuthal velocity profile remaining of solid body type, $v(r, z, t) = \Omega(z, t)r$, with an evolving angular velocity profile. Inspection of (1)–(4) suggests that if such a flow is mathematically feasible, the velocity field must satisfy the von Kármán–Bödewadt similarity principle:

$$u = rF(z, t), \qquad v = r\Omega(z, t), \qquad w = H(z, t). \tag{5}$$

According to this scaling, the vertical velocity field is independent of radius. Thus, all fluid comprising a horizontal surface is displaced vertically at the same rate, and initially horizontal material surfaces remain horizontal for all time. For the flows considered herein, the initially horizontal interface between vortices rotating with different angular velocities (or between a vortex overlying nonrotating air) remains horizontal. We note that the angular velocity Ω, the vertical vorticity $\zeta\,[\equiv(1/r)\partial rv/\partial r - (1/r)\partial u/\partial\phi = 2\Omega]$, and the horizontal divergence $\delta\,[\equiv(1/r)\partial ru/\partial r = 2F]$ are also independent of radius.

These similarity relations (without the time dependence) were used to describe steady-state flows induced by an infinite rotating disk (von Kármán 1921), the flow of a rotating fluid over a stationary disk (Bödewadt 1940), and flows between infinite rotating coaxial disks (Batchelor 1951; Stewartson 1953). The time-dependent relations were applied to the development of the von Kármán–Bödewadt flows by Pearson (1965), Bodonyi and Stewartson (1977), and Bodonyi (1978). Recent investigations into von Kármán–Bödewadt-type flows indicate the nonexistence of solutions as well as the existence of multiple solutions for certain parameter values (Zandbergen and Dijkstra 1987, and references therein).

In view of (4), F and the Stokes streamfunction ψ [defined by $u = (1/r)\partial\psi/\partial z$ and $w = (-1/r)\partial\psi/\partial r$] are related to H by

$$F = -\frac{1}{2}\frac{\partial H}{\partial z}, \tag{6}$$

$$\psi = -\frac{r^2}{2}H. \tag{7}$$

Using (5) and (6), the equations of motion (1)–(3) reduce to

$$\frac{r}{2}\left[-\frac{\partial}{\partial t}\left(\frac{\partial H}{\partial z}\right)+\frac{1}{2}\left(\frac{\partial H}{\partial z}\right)^2-H\frac{\partial^2 H}{\partial z^2}-2\Omega^2\right]=-\frac{1}{\rho}\frac{\partial p}{\partial r}, \quad (8)$$

$$\frac{\partial \Omega}{\partial t}=\Omega\frac{\partial H}{\partial z}-H\frac{\partial \Omega}{\partial z}, \quad (9)$$

$$\frac{\partial H}{\partial t}+H\frac{\partial H}{\partial z}=-\frac{1}{\rho}\frac{\partial p}{\partial z}. \quad (10)$$

Since the angular velocity Ω is half the vertical vorticity, the azimuthal equation of motion (9) can also be interpreted as the vertical vorticity equation. Equation (9) relates local changes in vertical vorticity to vertical advection and stretching of vertical vorticity.

An equation for the azimuthal vorticity component, η [$\equiv \partial u/\partial z - \partial w/\partial r = \partial u/\partial z = (-r/2)\partial^2 H/\partial z^2$], is obtained from the azimuthal component of the curl of the equations of motion. Taking $\partial/\partial r$ of (10), yields $\partial^2 p/\partial r \partial z = 0$, that is, the radial pressure gradient force is independent of height, a feature characteristic of boundary layer flows. In the context of geophysical vortices, however, the radial independence of the axial pressure gradient is an inadequacy of our similarity model (one shared by the stagnation-type Burgers, Rott, Sullivan, and Bellamy–Knights vortices and the viscous von Kármán–Bödewadt vortex flows). In view of this independence, the vertical derivative of (8) yields

$$\frac{\partial}{\partial z}\left[-\frac{\partial}{\partial t}\left(\frac{\partial H}{\partial z}\right)+\frac{1}{2}\left(\frac{\partial H}{\partial z}\right)^2-H\frac{\partial^2 H}{\partial z^2}-2\Omega^2\right]=0. \quad (11)$$

The azimuthal vorticity equation for axisymmetric, incompressible, inviscid flows is

$$\frac{\partial \eta}{\partial t}+u\frac{\partial \eta}{\partial r}+w\frac{\partial \eta}{\partial z}-u\frac{\eta}{r}-\frac{1}{r}\frac{\partial v^2}{\partial z}=0. \quad (12)$$

For a flow satisfying the similarity hypothesis (5), $u\partial\eta/\partial r$ and $-u\eta/r$ are of equal magnitude and opposite sign [$(\pm r/4)(\partial H/\partial z)(\partial^2 H/\partial z^2)$], and (12) splits into two equations that hold simultaneously,

$$\frac{\partial \eta}{\partial t}+w\frac{\partial \eta}{\partial z}-\frac{1}{r}\frac{\partial v^2}{\partial z}=0 \quad \text{and} \quad (13a)$$

$$u\frac{\partial \eta}{\partial r}-u\frac{\eta}{r}=0. \quad (13b)$$

According to (13a), local changes in azimuthal vorticity are forced by vertical advection of azimuthal vorticity and by differential centrifugal forcing. Equation (13b) describes a balance between the radial advection of azimuthal vorticity and the stretching of azimuthal vorticity associated with radially displaced toroidal vortex lines. It can readily be shown that (11) is equivalent to (13a).

Integrating (11) with respect to z gives back (8) with a function of integration $C(t)$ accounting for the radial pressure gradient force,

$$-\frac{\partial}{\partial t}\left(\frac{\partial H}{\partial z}\right)+\frac{1}{2}\left(\frac{\partial H}{\partial z}\right)^2-H\frac{\partial^2 H}{\partial z^2}-2\Omega^2=-C(t). \quad (14)$$

We can therefore think of (14) as either the vertically integrated azimuthal vorticity equation or as the radial equation of motion. Alternatively, we note that under the similarity hypothesis (5), the horizontal divergence equation (Brandes et al. 1988) reduces to

$$\frac{\partial \delta}{\partial t}+w\frac{\partial \delta}{\partial z}+\frac{\delta^2}{2}-\frac{\zeta^2}{2}=-\frac{1}{\rho}\nabla_H^2 p. \quad (15)$$

Applying $\zeta = 2\Omega$ and $\delta = -\partial H/\partial z$ in (15) yields (14), with $C(t)$ identified as $\nabla_H^2 p/\rho$. Thus (14) can also be interpreted as the divergence equation.

To determine the pressure, integrate (8) with respect to r, obtaining $p/\rho = Q(z, t) + C(t)r^2/4$. The function of integration $Q(z, t)$ is evaluated by applying this equation to (10) and integrating with respect to z. In this manner we find,

$$\frac{p}{\rho}=\frac{p_0}{\rho}-\left(\int_0^z \frac{\partial H}{\partial t}\,dz'+\frac{H^2}{2}\right)+C(t)\frac{r^2}{4}. \quad (16)$$

We will take $z = 0$ to be an impermeable boundary, in which case p_0 is the stagnation pressure. Here, $C(t)$, the height-independent forcing term in (14), is proportional to the radial pressure gradient force (and is equal to $\nabla_H^2 p/\rho$).

It should be noted that our two-dimensional (z, t) partial differential equations (9) and (14), and pressure formula (16) follow from the three-dimensional (r, z, t) Euler equations *without approximation.* The fact that radius does not appear in (9) or (14) confirms that exact solutions of the Euler equations in the similarity form (5) are at least mathematically feasible. In sections 3–5, we seek exact solutions of these equations for flows with piecewise constant vertical profiles of radial and angular velocity.

3. Governing equations for the *N*-layer vortex

We consider the special class of flows in which the azimuthal velocity is a piecewise constant function of height. In this case the azimuthal vorticity equation (12) can be expressed in Lagrangian form within each vortex layer as $d(\eta/r)/dt = \partial\Omega^2/\partial z = 0$, showing that η/r ($=\partial u/\partial z$) is conserved. If we consider the initial radial velocity field to be a piecewise function of height (so that $\partial u/\partial z = 0$ initially in a vortex layer), then η/r is zero initially, and the conservation principle indicates that η/r (and hence $\partial u/\partial z$) must be zero within each layer for all time (nonzero azimuthal vorticity is associated with infinite shear on the interfaces between the vortex layers). Thus, the radial velocity, angular momentum, and horizontal divergence are constant within each layer, and the vertical velocity varies linearly with height within each layer. In general, we consider N fluid layers in solid body rotation with different thicknesses

and rotation rates. We speculate that a vortex with a continuous profile of angular velocity should be well approximated by the discrete N layer model for large N.

With piecewise constant height dependencies for the azimuthal and radial velocity functions, and a piecewise linear height dependence for the vertical velocity function, the partial differential equations (9) and (14) [or equivalently (9) and (15)] reduce, without approximation, to a system of ordinary differential equations for the time-dependent amplitudes of the velocity functions. Low-order polynomials in the spatial coordinates (linear for velocity, quadratic for free-surface displacement) have been used previously to obtain exact solutions of the nonlinear shallow water equations corresponding to elliptic paraboloidal vortices and to free oscillations in rotating elliptic paraboloidal basins (Ball 1963; Miles and Ball 1963; Ball 1964 and 1965; Thacker 1981; Cushman-Roisin 1984 and 1987; Cushman-Roisin et al. 1985; Shapiro 1996). Numerical solutions of the shallow water equations with this polynomial model were employed by Tsonis et al. (1994) in a study of nonlinear time series analysis.

The vortex layers are labeled in order of increasing height, from the lowest layer ($n = 1$) to the highest layer ($n = N$). The nth layer thickness, angular momentum, and horizontal divergence functions are denoted by $T_n(t)$, $\Omega_n(t)$, and $\delta_n(t)$, respectively. The height of the $(n-1)$th interface (the interface between the $(n-1)$th and nth layers) is given by $z^*_{n-1} \equiv \sum_{i=1}^{n-1} T_i$. The nth vertical velocity function $H_n(z, t)$ is related to the horizontal divergence by $\delta_n(t) = -\partial H_n/\partial z$. Integrating this latter equation with respect to height within each layer yields $H_n(z, t) = -z\delta_n(t) + q_n(t)$, where $q_n(t)$ is the nth layer function of integration. Equivalently, we may write

$$\frac{dz}{dt} = -z\delta_n(t) + q_n(t), \qquad z \in [z^*_{n-1}, z^*_{n-1} + T_n). \tag{17}$$

Imposing the impermeability condition on the lower boundary ($z = 0$) yields $q_1 = 0$. The requirement that the vertical velocity be continuous across the layer interfaces then yields a recursion relation for the rest of the functions of integration, $q_n = q_{n-1} + z^*_{n-1}(\delta_n - \delta_{n-1})$. Thus, the vertical velocity field can be expressed completely in terms of the layer thicknesses and divergences.

With $\delta_n(t) = -\partial H_n/\partial z$, the vertical vorticity (azimuthal velocity) equation (9) becomes

$$\frac{d\Omega_n}{dt} = -\delta_n\Omega_n, \qquad n = 1, 2, \ldots, N, \tag{18}$$

and the divergence equation (15) becomes

$$\frac{d\delta_n}{dt} = -\frac{\delta_n^2}{2} + 2\Omega_n^2 - C(t), \qquad n = 1, 2, \ldots, N. \tag{19}$$

An equation for the evolution of the nth layer thickness $T_n(t)$ is obtained by evaluating (17) at the bottom and top of the nth layer (z^*_{n-1} and $z^*_{n-1} + T_n$, respectively) and subtracting the expression at the bottom from the expression at the top,

$$\frac{dT_n}{dt} = -\delta_n T_n, \qquad n = 1, 2, \ldots, N. \tag{20}$$

We suppose the flow is bounded from below by an impermeable boundary at $z = 0$ and consider two possible upper boundary conditions: (i) the flow is bounded at $z = h$ by an impermeable boundary or (ii) the flow is unbounded vertically, though with finite vertical velocity at vertical infinity (necessitating zero divergence in the top layer $\delta_N(t) = 0$). In the latter case, the top layer is displaced vertically, as a solid body, with no change in thickness ($dT_N/dt = 0$), and with a vertical velocity equal to the vertical velocity at the top of the underlying $(N-1)$th layer. According to the azimuthal equation of motion (18), the angular velocity in the top layer would then be unchanged [$\Omega_N(t) = \Omega_N(0)$], and the divergence equation (19) would yield

$$C(t) = 2\Omega_N^2 \quad \text{(for a vertically unbounded vortex)}. \tag{21}$$

In the case of the vertically bounded vortex, the total thickness of the vortex is constant,

$$\sum_{n=1}^{N} T_n = h, \quad \text{(for a vertically bounded vortex)}, \tag{22}$$

and therefore, $\sum_{n=1}^{N} dT_n/dt = 0$, or, in view of (20), $\sum_{n=1}^{N} \delta_n T_n = 0$.

Equations (18)–(20) compose $3N$ ordinary differential equations in $3N + 1$ unknowns: $T_n(t)$, $\Omega_n(t)$, $\delta_n(t)$, and $C(t)$ ($=\nabla_H^2 p/\rho$). Closure is provided by boundary data in the form of (21) [or, equivalently $\delta_N(t) = 0$] for the vertically unbounded vortex, or (22) for the bounded vortex.

A first integral of the motion is obtained by eliminating δ_n between (18) and (20), resulting in the nth-layer potential vorticity conservation equation, $d(\Omega_n/T_n)/dt = 0$, or

$$\frac{\Omega_n(t)}{T_n(t)} = \frac{\Omega_n(0)}{T_n(0)}, \qquad n = 1, 2, \ldots, N. \tag{23}$$

Since $T_n(t) > 0$, the rotation rate $\Omega_n(t)$ is always of the same sense as the initial rotation rate $\Omega_n(0)$.

Eliminating C(t) from Eq. (19) as applied to the nth and $(n-1)$th layers yields $N - 1$ equations of the form

$$\frac{d\delta_n}{dt} - \frac{d\delta_{n-1}}{dt} + \frac{\delta_n^2}{2} - \frac{\delta_{n-1}^2}{2} - 2\Omega_n^2 + 2\Omega_{n-1}^2 = 0, \qquad n = 2, 3, \ldots, N. \tag{24}$$

Using (20) and (23) to eliminate δ_n, δ_{n-1}, Ω_n, and Ω_{n-1} in (24) in favor of the layer thicknesses, we get $N - 1$ coupled second-order equations in N unknowns,

$$\frac{1}{T_{n-1}}\frac{d^2T_{n-1}}{dt^2} - \frac{1}{T_n}\frac{d^2T_n}{dt^2} - \frac{3}{2}\left(\frac{1}{T_{n-1}}\frac{dT_{n-1}}{dt}\right)^2 + \frac{3}{2}\left(\frac{1}{T_n}\frac{dT_n}{dt}\right)^2 + 2\left(\frac{\Omega_{n-1}(0)}{T_{n-1}(0)}\right)^2 T_{n-1}^2 - 2\left(\frac{\Omega_n(0)}{T_n(0)}\right)^2 T_n^2 = 0, \quad n = 2, 3, \ldots, N. \tag{25}$$

Closure is provided by the boundary data, as described above.

4. Two-layer vortices

a. Vortex overlying nonrotating fluid—Rigid lower boundary

First consider the special case of a solid body vortex of infinite radial and vertical extent overlying nonrotating fluid bounded from below by a rigid horizontal plate. The initial radial and vertical velocity components in both layers are taken to be zero. After the initial time, the vortex pressure gradient (which is impressed on the nonrotating fluid) induces a radial inflow in the nonrotating fluid. Associated with this converging low-level flow is a horizontally uniform vertical velocity field that increases in magnitude with height from the lower boundary up to the vortex/nonrotating fluid interface. Since there is no upper boundary, the vertical motion in the vortex should not be impeded, and the vortex can be displaced upward, as a solid body, with zero radial velocity and with a vertical velocity equal to the vertical velocity at the interface. According to the azimuthal equation of motion (18), the angular velocity in the vortex Ω_2 would be unchanged by the upward displacement, and the azimuthal velocity in the lower fluid would be zero since it was zero initially. Thus, our special case corresponds to $N = 2$, $\zeta_1 \equiv 0$, and $\delta_2 \equiv 0$. From (21), $C(t)$ is equal to $2\Omega_2^2$, a positive constant, and the divergence equation (19) for the nonrotating layer ($n = 1$) becomes

$$\frac{d\delta_1}{dt} = -\frac{\delta_1^2}{2} - 2\Omega_2^2, \tag{26}$$

which has the general solution

$$\delta_1 = -2\Omega_2\left(\frac{\sin\Omega_2 t - B\cos\Omega_2 t}{\cos\Omega_2 t + B\sin\Omega_2 t}\right). \tag{27}$$

The initial condition $\delta_1(0) = 0$ implies that $B = 0$, and (27) reduces to

$$\delta_1 = -2\Omega_2 \tan\Omega_2 t. \tag{28}$$

The thickness of the nonrotating layer (interface height) is obtained from (20) and (28) as

$$T_1(t) = T_1(0)\sec^2\Omega_2 t. \tag{29}$$

Thus, the divergence (and the radial and vertical velocity components) and the interface height increase rapidly and become infinite at a finite time, $T = \pi/(2\Omega_2)$, equal to a quarter of the orbital period $T^* (= 2\pi/\Omega_2)$ of upper-layer parcels about the axis of symmetry.[1] This intriguing result can be compared with the singular behavior of some unsteady viscous von Kármán–Bödewadt-type flows. Bodonyi (1978) and Bodonyi and Stewartson (1977) report a breakdown of the numerical solution (verified by an asymptotic analysis) of rotating flow in which a lower disk is abruptly forced to counterrotate. In these studies the velocity field and boundary layer depth on the lower disk grew explosively and became singular within half an orbital period. We speculate that the breakdown mechanism for the viscous counterrotating flow is similar to that in our inviscid elevated vortex flow: in the absence of an upper boundary, the maintained impressing of a vortex pressure gradient force on nonrotating fluid leads to explosive vertical accelerations. In the context of our inviscid elevated vortex, a nonrotating fluid layer is specified in the initial condition. In the viscous counterrotating flows, a level of nonrotating fluid (the exact location of which is influenced by diffusion) is always present.

b. Two layer vortices—Rigid lower boundary

If the lower fluid has some rotation, no matter how small, the singular behavior deduced above disappears. Instead, an oscillatory secondary circulation is set up in the flow in which the angular velocity and thickness of the lower-layer vortex alternately increases and decreases. In the absence of an upper rigid lid, the elevated vortex oscillates vertically as a solid body ($\Omega_2 = \text{const}$, $\delta_2 \equiv 0$).

For the lower-layer flow ($n = 1$), (19), (20), and (23) become

$$\frac{d\delta_1}{dt} + \frac{\delta_1^2}{2} + 2\Omega_2^2 - 2\Omega_1^2 = 0, \tag{30}$$

$$\delta_1(t) = -\frac{1}{T_1}\frac{dT_1}{dt}, \tag{31}$$

$$\Omega_1(t) = \frac{\Omega_1(0)}{T_1(0)}T_1(t). \tag{32}$$

Applying (31) and (32) in (30) results in a second-order nonlinear ordinary differential equation for the lower-layer thickness (interface height),

[1] It can also be shown that the flow becomes singular within a finite time for (i) $\Omega_2 \neq 0$ and any choice of initial value $\delta_1(0)$, and for (ii) $\Omega_2 = 0$ and any negative initial value $\delta_1(0)$. In either case, the singularity is associated with the nonlinear term δ_1^2 in (26), or, equivalently, the $(\partial H/\partial z)^2$ term in (8), which accounts for radial advection of radial momentum.

$$\frac{d^2T_1}{dt^2} - \frac{3}{2}\frac{1}{T_1}\left(\frac{dT_1}{dt}\right)^2 + 2\left(\frac{\Omega_1(0)}{T_1(0)}\right)^2 T_1^3 = 2\Omega_2^2 T_1. \quad (33)$$

Since (33) does not explicitly involve the independent variable, its order may be reduced by changing the dependent variable to $P \equiv dT_1/dt$ and regarding T_1 as the new independent variable,

$$\frac{dP^2}{dT_1} - 3\frac{P^2}{T_1} + 4\left(\frac{\Omega_1(0)}{T_1(0)}\right)^2 T_1^3 = 4\Omega_2^2 T_1. \quad (34)$$

Equation (34) is a first-order linear equation for P^2, with solution (subject to the condition of no initial vertical motion),

$$\left(\frac{dT_1}{dt}\right)^2 = -4\left(\frac{\Omega_1(0)}{T_1(0)}\right)^2 T_1^4 + 4\left(\frac{\Omega_1^2(0)}{T_1(0)} + \frac{\Omega_2^2}{T_1(0)}\right)T_1^3 - 4\Omega_2^2 T_1^2,$$

or, after taking the root,

$$\frac{dT_1}{dt} = \pm 2\frac{|\Omega_1(0)|}{T_1(0)} T_1 \left\{[T_1 - T_1(0)]\left[\frac{\Omega_2^2 T_1(0)}{\Omega_1^2(0)} - T_1\right]\right\}^{1/2}. \quad (35)$$

The sign in (35) is determined by the requirement that the solution be real, that is, that $[T_1 - T_1(0)][\Omega_2^2 T_1(0) - \Omega_1^2(0)T_1]$ be nonnegative. If upper-vortex rotation is initially greater in magnitude than lower-vortex rotation $[\Omega_2^2 - \Omega_1^2(0) > 0]$, the solution must initially proceed such that $T_1 - T_1(0) > 0$, that is, the positive branch must be chosen and the interface rises. Conversely, if upper-vortex rotation is initially smaller in magnitude than lower-vortex rotation $[\Omega_2^2 - \Omega_1^2(0) < 0]$, the solution initially proceeds on the negative branch and the interface falls. Therefore, the $\pm$ symbol may be replaced with $[\Omega_2^2 - \Omega_1^2(0)]/|\Omega_2^2 - \Omega_1^2(0)|$.

Separating variables in (35), integrating, and applying the initial condition yields

$$\sin^{-1}\left[\frac{[\Omega_2^2 + \Omega_1^2(0)]T_1 - 2\Omega_2^2 T_1(0)}{T_1|\Omega_2^2 - \Omega_1^2(0)|}\right] = \frac{\Omega_2^2 - \Omega_1^2(0)}{|\Omega_2^2 - \Omega_1^2(0)|}\left(2\Omega_2 t - \frac{\pi}{2}\right), \quad (36)$$

or, after rearrangement,

$$T_1 = \frac{2T_1(0)}{1 + \alpha + (1 - \alpha)\cos 2\Omega_2 t}, \quad (37)$$

where $\alpha \equiv \Omega_1^2(0)/\Omega_2^2$ is the ratio of the (squared) lower-layer to upper-layer angular velocities. Applying (37) in (31) and (32), we obtain δ_1 and Ω_1 as

$$\delta_1 = -\frac{2\Omega_2(1 - \alpha)\sin 2\Omega_2 t}{1 + \alpha + (1 - \alpha)\cos 2\Omega_2 t}, \quad (38)$$

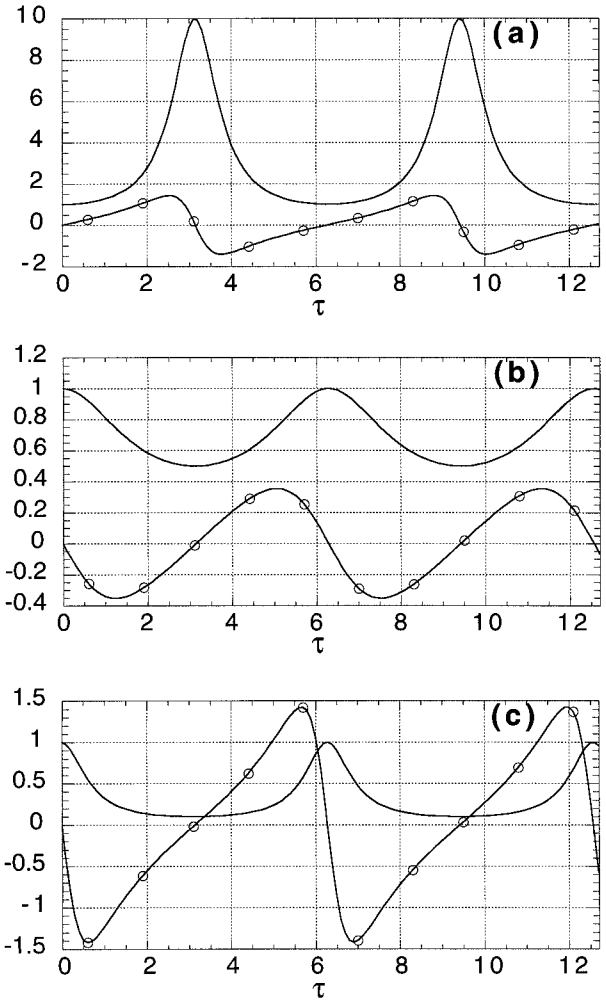

FIG. 1. Evolution of nondimensional interface height $T_1/T_1(0)$ (solid line) and lower layer convergence $-\delta_1/2|\Omega_2|$ (line with circles) for the vertically unconfined two-layer vortex with (a) $\alpha = 0.1$, (b) $\alpha = 2.0$, and (c) $\alpha = 10.0$. The lower-layer radial velocity function is given by $F_1 = \delta_1/2$. Here $\alpha \equiv \Omega_1^2(0)/\Omega_2^2$ is the initial ratio of (squared) lower-layer to upper-layer angular velocity, and $\tau \equiv 2|\Omega_2|t$ is nondimensional time.

$$\Omega_1 = \frac{2\Omega_1(0)}{1 + \alpha + (1 - \alpha)\cos 2\Omega_2 t}. \quad (39)$$

In contrast to the singular nature of a vertically unbounded elevated vortex overlying nonrotating fluid, the two-layer vortex is well behaved for all time (see Fig. 1). Here the converging ''in-up'' flow induced in the lower layer by the upper-layer vortex spins up the weak vertical vorticity in the lower layer. Eventually the lower-layer vortex becomes stronger than the upper-layer vortex and the vertical pressure gradient force reverses. In response, the secondary circulation reverses and the lower-layer vortex spins down, eventually becoming weaker than the upper-layer vortex. The process repeats itself and we obtain an oscillation of the interface height and lower-layer vortex strength.

The period of these oscillations, $T = \pi/|\Omega_2|$, is half the orbital period of parcels in the upper vortex. It can be inferred from (35) or (37) that the interface height T_1 oscillates vertically between levels $T_1(0)$ and $T_1(0)\Omega_2^2/\Omega_1^2(0)$. Thus, the amplitude of the interface oscillation increases sharply with decreasing initial rotation in the lower level. For the case of strong initial lower-level rotation, the interface height rapidly drops to a small value and maintains small values throughout much of the oscillation period.

c. Two-layer vortices—Rigid upper and lower boundaries

Now suppose that impermeable horizontal boundaries confine the flow on the bottom ($z = 0$) and at the top ($z = h$). Both layers of this two-layer vortex are initially in solid body rotation with different (nonzero) angular velocities and no initial secondary circulation. The special case of a vortex overlying nonrotating fluid is examined in section 4d.

Setting $n = 2$ in (24) yields

$$\frac{d\delta_2}{dt} - \frac{d\delta_1}{dt} + \frac{\delta_2^2}{2} - \frac{\delta_1^2}{2} - 2\Omega_2^2 + 2\Omega_1^2 = 0. \quad (40)$$

Equations (20) and (23) for $n = 1, 2$ become

$$\delta_1 = -\frac{1}{T_1}\frac{dT_1}{dt}, \qquad \delta_2 = \frac{1}{h - T_1}\frac{dT_1}{dt}, \quad (41a,b)$$

$$\Omega_1(t) = \frac{\Omega_1(0)}{T_1(0)}T_1(t), \qquad \Omega_2(t) = \frac{\Omega_2(0)}{h - T_1(0)}[h - T_1(t)], \quad (42a,b)$$

where we have used $T_2 = h - T_1$ [obtained from (22)].

Applying (41a,b) and (42a,b) in (40) yields a second-order nonlinear ordinary differential equation for the interface height,

$$\frac{d^2T_1}{dt^2} + \frac{3}{2}\left(\frac{1}{h - T_1} - \frac{1}{T_1}\right)\left(\frac{dT_1}{dt}\right)^2 - 2\frac{T_1}{h}\left[\frac{\Omega_2(0)}{h - T_1(0)}\right]^2(h - T_1)^3 + 2\frac{T_1^3}{h}\left[\frac{\Omega_1(0)}{T_1(0)}\right]^2(h - T_1) = 0.$$

Again, changing the dependent variable to $P \equiv dT_1/dt$ and regarding T_1 as the new independent variable yields a first-order linear equation for P^2:

$$\frac{dP^2}{dT_1} + 3\left(\frac{1}{h - T_1} - \frac{1}{T_1}\right)P^2 - 4\frac{T_1}{h}\left[\frac{\Omega_2(0)}{h - T_1(0)}\right]^2(h - T_1)^3 + 4\frac{T_1^3}{h}\left[\frac{\Omega_1(0)}{T_1(0)}\right]^2(h - T_1) = 0. \quad (43)$$

Solving (43) subject to the initial condition $P(0) = 0$, we obtain:

$$\left(\frac{dT_1}{dt}\right)^2 = \frac{4}{h}T_1^2(h - T_1)^2[T_1 - T_1(0)] \times \left\{\left[\frac{\Omega_2(0)}{h - T_1(0)}\right]^2\frac{(h - T_1)}{T_1(0)} - \left[\frac{\Omega_1(0)}{T_1(0)}\right]^2\frac{T_1}{h - T_1(0)}\right\}. \quad (44)$$

The qualitative behavior of $T_1(t)$ can be deduced with analogy to one-dimensional particle motion in a potential field, that is, by regarding T_1 as a particle displacement and (44) as an energy equation for a conservative system. We regard $(dT_1/dt)^2$ as the kinetic energy and the right-hand side of (44) as (the negative of) a nonlinear potential energy function. Since $(dT_1/dt)^2$ is nonnegative, the right-hand side must be nonnegative on any domain of physical interest. The behavior of the solution depends on the nature of this nonlinear potential energy, especially on the points for which the potential energy vanishes. These points are local extrema of $T_1(t)$, and represent the turning points of the differential equation. These extrema can be identified as $T_1 = T_1(0)$, h, and T_1', where

$$T_1' \equiv h\left\{1 + \left[\frac{h}{T_1(0)} - 1\right]\left[\frac{\Omega_1(0)}{\Omega_2(0)}\right]^2\right\}^{-1}. \quad (45)$$

It is straightforward to show that if $|\Omega_2(0)| < |\Omega_1(0)|$, then $0 < T_1' < T_1(0)$, whereas if $|\Omega_2(0)| > |\Omega_1(0)|$, then $h > T_1' > T_1(0)$. If the lower layer is not rotating [$\Omega_1(0) = 0$], then $T_1' = h$, whereas if the upper layer is not rotating [$\Omega_2(0) = 0$], then $T_1' = 0$. We consider the case where neither $\Omega_1(0)$ nor $\Omega_2(0)$ are zero. Taking the root of (44) yields

$$\frac{dT_1}{dt} = \pm 2|\Omega_2(0)|\left[\frac{h - T_1}{h - T_1(0)}\right] \times T_1\left\{\frac{(T_1' - T_1)[T_1 - T_1(0)]}{T_1'T_1(0)}\right\}^{1/2}, \quad (46)$$

where the choice of sign is determined by the requirement that the solution be real, that is, that $[T_1' - T_1][T_1 - T_1(0)]$ be nonnegative. If upper-layer rotation is initially stronger than lower-layer rotation [so that $T_1' - T_1(0) > 0$], the solution must proceed initially on the positive branch of (46) and the interface rises, whereas if upper-layer rotation is initially weaker than lower-layer rotation [so that $T_1' - T_1(0) < 0$], the solution must proceed initially on the negative branch of (46) and the interface falls. Thereafter, in either case, the sign in (46) changes each time T_1 reaches a turning point. The solution is such that T_1 oscillates between $T_1(0)$ and T_1'. The solution first reaches the turning point $T_1 = T_1'$ at $t = T/2$ and completes one period of oscillation at $t = T$, when T_1 returns to $T_1(0)$.

The solution is obtained by separating variables in (46) and integrating,

$$\int \frac{dT_1}{T_1(h - T_1)\{[T_1 - T_1(0)][T_1' - T_1]\}^{1/2}} = \frac{2\ \mathrm{sgn}[T_1' - T_1(0)]|\Omega_2(0)|}{[T_1'T_1(0)]^{1/2}[h - T_1(0)]} \int dt, \tag{47}$$

where sgn is the unit sign function: $\mathrm{sgn}[T_1' - T_1(0)] = 1$ for $T_1' > T_1(0)$, $= -1$ for $T_1' < T_1(0)$. A partial fractions decomposition puts the left-hand side of (47) in the form of tabulated integrals. The constant of integration is determined piecewise (constant for each half-period) by considering the initial condition and the continuity of $T_1(t)$ at the turning points. Thus, we obtain the implicit solution for $T_1(t)$ over a period T of this oscillation as

$$\frac{2|\Omega_2(0)|h}{[h - T_1(0)]}t = \frac{\pi}{2} + \frac{\pi}{2}\left\{\frac{T_1'T_1(0)}{[h - T_1(0)](h - T_1')}\right\}^{1/2} + \Phi[T_1, T_1(0), T_1'], \tag{48}$$

as T_1 travels from $T_1(0)$ to T_1' $(0 < t \leq T/2)$, and

$$\frac{2|\Omega_2(0)|h}{[h - T_1(0)]}\left(\frac{T}{2} - t\right) = -\frac{\pi}{2} - \frac{\pi}{2}\left\{\frac{T_1'T_1(0)}{[h - T_1(0)](h - T_1')}\right\}^{1/2} + \Phi(T_1, T_1(0), T_1'), \tag{49}$$

as T_1 travels from T_1' back to $T_1(0)$ $(T/2 < t < T)$, where

$$\Phi[T_1, T_1(0), T_1'] = \sin^{-1}\left\{\frac{[T_1' + T_1(0)]T_1 - 2T_1'T_1(0)}{T_1[T_1' - T_1(0)]}\right\} - \left\{\frac{T_1'T_1(0)}{[h - T_1(0)](h - T_1')}\right\}^{1/2} \sin^{-1}\left\{\frac{[2h - T_1(0) - T_1'](h - T_1) - 2[h - T_1(0)](h - T_1')}{(h - T_1)[T_1' - T_1(0)]}\right\}. \tag{50}$$

The oscillation period is

$$T = \frac{\pi[h - T_1(0)]}{h|\Omega_2(0)|}\left\langle 1 + \left\{\frac{T_1'T_1(0)}{[h - T_1(0)](h - T_1')}\right\}^{1/2}\right\rangle. \tag{51}$$

Applying (45) to (51), the oscillation period becomes

$$T = \pi\left\{\frac{1}{|\Omega_2(0)|}\left[1 - \frac{T_1(0)}{h}\right] + \frac{1}{|\Omega_1(0)|}\frac{T_1(0)}{h}\right\} = \frac{\pi}{h}\int_0^h \frac{1}{|\Omega(z, 0)|}\, dz. \tag{52}$$

Thus T is equal to π times the mean reciprocal magnitude of the initial angular velocity, or half the mean initial orbital period.

Solutions for Ω_1 and Ω_2 in terms of the interface height follow immediately from (42a,b). Solutions for δ_1 and δ_2 are obtained from (41a,b) and (46)

$$\delta_1 = \mp 2|\Omega_2(0)|\left[\frac{h - T_1}{h - T_1(0)}\right]\left\{\frac{(T_1' - T_1)[T_1 - T_1(0)]}{T_1'T_1(0)}\right\}^{1/2}, \tag{53}$$

$$\delta_2 = \pm 2|\Omega_2(0)|\left[\frac{T_1}{h - T_1(0)}\right]\left\{\frac{(T_1' - T_1)[T_1 - T_1(0)]}{T_1'T_1(0)}\right\}^{1/2}, \tag{54}$$

the signs being inferred piecewise (on half-period intervals) from the above considerations.

Two examples are presented in Fig. 2. In both cases the initial interface height $T_1(0)$ is set at $0.2h$. In Fig. 2a the lower-layer rotation is initially weaker than the upper-layer rotation and the interface quickly rises (thus strengthening the lower-layer angular velocity and sowing the seeds for the eventual reversal of the secondary circulation). The interface rapidly displaces much of the upper-layer fluid and maintains a high altitude throughout much of the period. In the case of strong low-layer rotation [Fig. 2(b)], the interface initially falls. Despite the gentleness of the interface descent, a jet of strong radial velocity appears in the lower layer, a consequence of mass conservation and the relative shallowness of the lower layer.

d. Vortex overlying nonrotating fluid—Rigid upper and lower boundaries

If there is no rotation in the lower layer initially, $\Omega_1(0) = 0$, and therefore $\Omega_1(t) = 0$ for all time and $T_1' = h$. In this case, we need only consider the positive branch of (46). Separating variables and integrating, we obtain,

$$\sin^{-1}\left\{\frac{[h + T_1(0)]T_1 - 2hT_1(0)}{T_1[h - T_1(0)]}\right\} + \frac{2[hT_1(0)]^{1/2}}{h - T_1(0)}\left[\frac{T_1 - T_1(0)}{h - T_1}\right]^{1/2} = -\frac{\pi}{2} + \frac{2h|\Omega_2(0)|}{h - T_1(0)}t. \tag{55}$$

The solution for Ω_2 follows from (42), and the solutions for δ_1 and δ_2 are given by the negative and positive branches of (53) and (54), respectively, with $T_1(t)$ de-

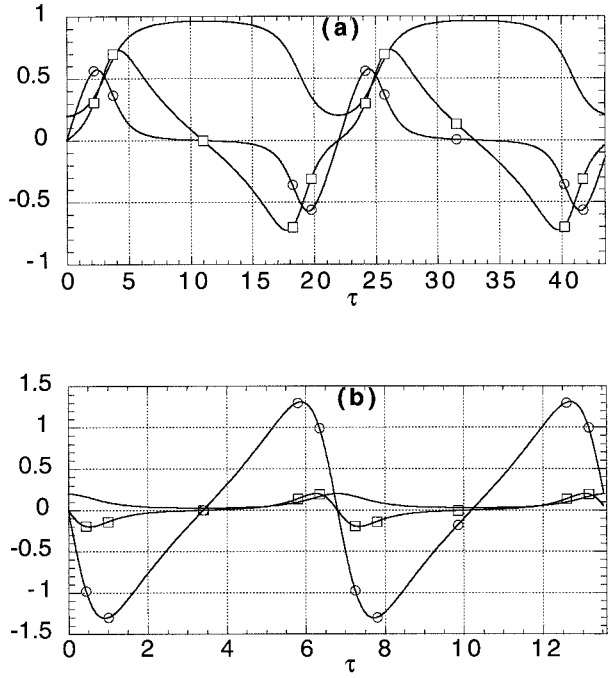

FIG. 2. Evolution of a vertically confined two-layer vortex. Nondimensional interface height T_1/h (solid line), lower-layer convergence $-\delta_1/2|\Omega_2|$ (line with circles), and upper-layer divergence $\delta_2/2|\Omega_2|$ (line with squares) are shown for an initial interface height $T_1(0)$ of $0.2h$. Initial ratio of lower-layer to upper-layer angular velocities $\Omega_1(0)/\Omega_2(0)$ is (a) 0.1 and (b) 3.0. The radial velocity function is given by $F_1 = \delta_1/2$ in the lower layer and $F_2 = \delta_2/2$ in the upper layer. The angular velocity functions are proportional to the respective layer thicknesses. Here $\tau \equiv [2h|\Omega_2(0)|]/[h - T_1(0)]t$ is nondimensional time.

termined implicitly from (55). The solution, depicted in Fig. 3 for $T_1(0) = 0.2h$, shows a period of rapid initial interface ascent followed by a long period of gentle ascent. The slowness of the radial velocity decay in the top layer is again a consequence of mass conservation and the thinness of that layer. Since there is no vertical vorticity in the lower layer, the stretching mechanism does not operate and there is no mechanism to reverse the sense of the secondary circulation.

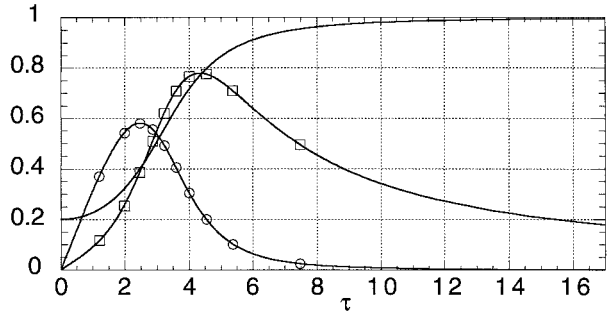

FIG. 3. Evolution of a vertically confined vortex overlying nonrotating fluid. Nondimensional interface height T_1/h (solid line), lower-layer convergence $-\delta_1/2|\Omega_2|$ (line with circles), and upper-layer divergence $\delta_2/2|\Omega_2|$ (line with squares) are shown for an initial interface height $T_1(0)$ of $0.2h$. The radial velocity function is given by $F_1 = \delta_1/2$ in the lower layer and $F_2 = \delta_2/2$ in the upper layer. The angular velocity function in the upper layer is proportional to the upper-layer thickness. Here $\tau \equiv [2h|\Omega_2(0)|]/[h - T_1(0)]$t is nondimensional time.

e. Invariance—Three-layer and multiple-layer planar-symmetric vortices

Equations (8)–(10) are invariant to the transformation: $z \to -z$, $H \to -H$. Therefore, from symmetry considerations, the two-layer solutions described above can be reflected about the lower impermeable boundary, $z = 0$, to produce analytic three-layer solutions,

$$u(r, -z, t) = u(r, z, t), \tag{56}$$

$$v(r, -z, t) = v(r, z, t), \tag{57}$$

$$w(r, -z, t) = -w(r, z, t). \tag{58}$$

In the case of the semi-infinite two-layer vortices confined by a lower boundary, a reflection of the solution results in an unconfined three-layer vortex solution defined piecewise on the vertical intervals, $z \in (-\infty, -T_1)$, $z \in (-T_1, T_1)$, and $z \in (T_1, \infty)$. In the case of two-layer vortices confined between horizontal boundaries at $z = 0$ and $z = h$, a reflection of the solution results in a confined three-layer vortex solution defined piecewise on the vertical intervals, $z \in (-h, -T_1)$, $z \in (-T_1, T_1)$, and $z \in (T_1, h)$. Further reflections of these confined vortices about the new boundaries are possible and lead to new planar-symmetric multiple-layer vortex solutions. Apart from their own intrinsic interest, these analytic solutions can also be used to validate the numerical algorithms for the more general (asymmetric) multiple-layer vortices described in the next section.

5. Numerical solutions for three-layer vortices

The behavior of three-layer vortices follows from the solution of (25) and (22) with $N = 3$. It is convenient to nondimensionalize variables as

$$\tilde{T}_1 \equiv \frac{T_1}{h}, \qquad \tilde{T}_2 \equiv \frac{T_2}{h}, \qquad \tau \equiv \overline{\Omega}t,$$

$$\frac{1}{\overline{\Omega}} \equiv \frac{\tilde{T}_1(0)}{|\Omega_1(0)|} + \frac{\tilde{T}_2(0)}{|\Omega_2(0)|} + \frac{\tilde{T}_3(0)}{|\Omega_3(0)|}, \tag{59}$$

where $\tilde{T}_3 = 1 - \tilde{T}_1 - \tilde{T}_2$, and rewrite (25) as a system of four coupled first-order equations,

$$\frac{d\tilde{T}_1}{d\tau} = P, \tag{60}$$

$$\frac{d\tilde{T}_2}{d\tau} = Q, \tag{61}$$

$$\frac{dP}{d\tau} = \tilde{T}_1(1 - \tilde{T}_1)A - \tilde{T}_1\tilde{T}_2 B, \tag{62}$$

$$\frac{dQ}{d\tau} = -\tilde{T}_1\tilde{T}_2 A + \tilde{T}_2(1 - \tilde{T}_2)B, \tag{63}$$

where

$$A \equiv \frac{3}{2}\left[\left(\frac{P}{\tilde{T}_1}\right)^2 - \left(\frac{P + Q}{1 - \tilde{T}_1 - \tilde{T}_2}\right)^2\right] - \alpha\tilde{T}_1^2 + \gamma(1 - \tilde{T}_1 - \tilde{T}_2)^2, \tag{64}$$

$$B \equiv \frac{3}{2}\left[\left(\frac{Q}{\tilde{T}_2}\right)^2 - \left(\frac{P + Q}{1 - \tilde{T}_1 - \tilde{T}_2}\right)^2\right] - \beta\tilde{T}_2^2 + \gamma(1 - \tilde{T}_1 - \tilde{T}_2)^2, \tag{65}$$

$$\alpha \equiv 2\left(\frac{\Omega_1(0)/\overline{\Omega}}{\tilde{T}_1(0)}\right)^2, \qquad \beta \equiv 2\left(\frac{\Omega_2(0)/\overline{\Omega}}{\tilde{T}_2(0)}\right)^2,$$

$$\gamma \equiv 2\left(\frac{\Omega_3(0)/\overline{\Omega}}{1 - \tilde{T}_1(0) - \tilde{T}_2(0)}\right)^2. \tag{66}$$

By definition, $1/\overline{\Omega}$ is proportional to the sum of the reciprocal potential vorticities in the three layers, while α, β, and γ are proportional to the squared potential vorticities in the lower, middle, and upper layers, respectively. These definitions imply

$$\left(\frac{2}{\alpha}\right)^{1/2} + \left(\frac{2}{\beta}\right)^{1/2} + \left(\frac{2}{\gamma}\right)^{1/2} = 1, \tag{67}$$

so that only two of α, β, and γ are independent. However, rather than specifying α, β, γ, and $\overline{\Omega}$ directly (and then deriving the initial angular velocity functions), we found it convenient to calculate α, β, γ, and $\overline{\Omega}$ from specified values of $\tilde{T}_1(0)$, $\tilde{T}_2(0)$, $\Omega_1(0)$, $\Omega_2(0)$, and $\Omega_3(0)$. It can be noted that if $\Omega_1(0)$, $\Omega_2(0)$, and $\Omega_3(0)$ undergo proportional changes [so that the ratios $\Omega_1(0)/\Omega_2(0)$ and $\Omega_1(0)/\Omega_3(0)$ are preserved], $\overline{\Omega}$ changes while α, β, and γ remain the same. Thus, the shape of the solution curve is affected by the relative magnitudes of the rotation rates while the timescale is affected by the mean rotation rate (as measured by $\overline{\Omega}$).

Equations (60)–(63) were integrated numerically for a variety of initial conditions with the fourth-order Runge–Kutta formula (Press et al. 1992). In each case the integrations were performed from $\tau = 0$ to $\tau = 15$ with a nondimensional time step size $\Delta\tau = 0.01$. A variety of interesting waveforms were obtained by varying the parameter settings, but in all cases the solutions were periodic. We speculate that the three-layer vortex is nonchaotic but that chaos might be possible in vortices with more layers. Results from selected three-layer calculations are depicted in Figs. 4–7. In these cases the three layers are initially of equal thickness: $\tilde{T}_1(0) = \tilde{T}_2(0) = 1 - \tilde{T}_1(0) - \tilde{T}_2(0) = \frac{1}{3}$. The parameter settings are given in Table 1.

In vortex A1:2:4 (Fig. 4) the initial angular velocity functions are specified to increase upward in a ratio of 1:2:4. There is no initial vertical motion [$P(0) = Q(0) = 0$]. As in the two-layer case, the initially weakest vortex layer (low layer in this case) rapidly thickens during the first half of the oscillation period and increases its angular velocity, while the initially strongest vortex layer (upper layer) rapidly thins and weakens its angular velocity. The layer of middle strength rotation (middle layer) thickens slightly at first but then thins. The motion of the interfaces during the first half of the oscillation period is associated with an in-up-out secondary circulation in which the lowest layer participates in the inflow and the upper layer participates in the outflow. The middle layer first participates in the inflow and then participates in the outflow. The sense of the circulation reverses for all layers halfway through the oscillation period. Vortex B1:2:10 (Fig. 5) is similar to vortex A1:2:4 except the initial angular velocities now increase upward in a ratio of 1:2:10. The increased initial discrepancy between the rotation rates in the lowest two layers and the upper layer amplifies the subsequent secondary circulation in all layers. Next consider vortex C1:2:4 (Fig. 6), which has an initially descending upper interface with a vertical velocity of $Q(0) = -0.5$ (all other initial conditions being the same as in A1:2:4). Introduction of the nonzero interface velocity creates an asymmetry in the waveforms of all the variables. Compared to A1:2:4, we see that the initial descent of the upper-layer interface in C1:2:4 results in a short-term increase in the upper-layer thickness and a decrease in the middle-layer thickness. However, the lower layer, responding to the vortex pressure gradient, thickens as in A1:2:4. Vortex D1:2:10, the counterpart of B1:2:10 with nonzero initial vertical velocity $Q(0) = -0.5$, is depicted in Fig. 7.

6. Initial behavior of an elevated vortex with radial power-law decay for $r > R$

The similarity vortices in sections 2–5 are noteworthy in that they provide rare exact descriptions of nonlinear interactions between vortex circulations and vortex-induced secondary circulations. However, the restrictive nature of the similarity scalings for the velocity and pressure fields suggest that the relevance of the similarity solutions to geophysical flows may be limited to the interior portions of broad vortices. Although the general validity of the similarity approach to solid body vortices of finite area lies beyond the scope of this investigation, a specific comparison at a small time is provided later in this section.

Mid- and lower-level mesocyclones and other me-

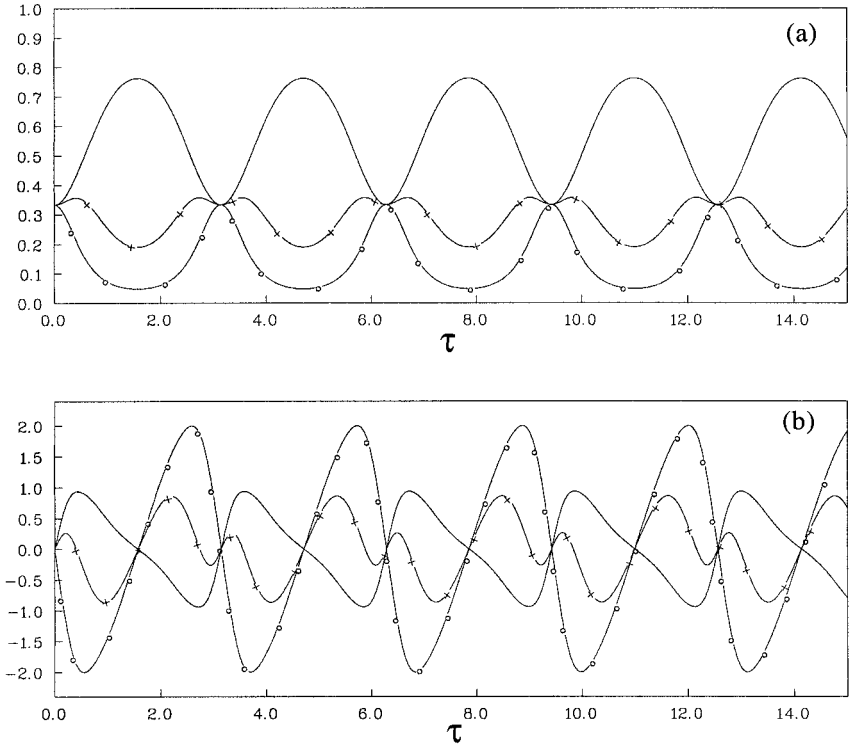

FIG. 4. Evolution of vortex A1:2:4, a vertically confined three-layer vortex with initially equal layer thicknesses, and initial layer angular velocities increasing upward in a ratio of 1:2:4. The two interfaces have no initial vertical motion. (a) Nondimensional lower-layer thickness $\tilde{T}_1$ (solid line), middle-layer thickness $\tilde{T}_2$ (line with plus symbols), and upper-layer thickness $\tilde{T}_3 = 1 - \tilde{T}_1 - \tilde{T}_2$ (line with circles). (b) Nondimensional convergence values $-\delta_1/\overline{\Omega}$, $-\delta_2/\overline{\Omega}$, and $-\delta_3/\overline{\Omega}$ in the lower (solid line), middle (line with plus symbols), and upper layers (line with circles), respectively. The nth layer radial velocity function is given by $F_n = \delta_n/2$ for $n = 1, 2, 3$. The angular velocity functions are proportional to the respective layer thicknesses. Here $\tau \equiv \overline{\Omega}t$ is nondimensional time.

soscale geophysical vortices typically consist of an isolated region of large vorticity embedded within a more-or-less nonrotating larger-scale environment. It is therefore of interest to study a solid body-type vortex of finite area embedded within a radially decaying vortex. As before, we consider our vortex to be elevated, that is, both inner and outer parts of the vortex overlie a layer of nonrotating fluid. There is no initial secondary circulation in either the vortex or the lower fluid.

The length scale associated with a finite vortex core greatly complicates the analysis and we abandon our search for exact solutions. Instead, we present a linear analysis of the flow appropriate for small times. The long-term behavior will be investigated in future numerical simulations.

Consider a vortex with an initial azimuthal velocity distribution v^0 [$\equiv v(r, z, 0)$] given by

$$v^0(r, z) = \begin{cases} \Omega r, & r \le R, \quad T_1 \le z \le h, \\ \Omega R\left(\dfrac{R}{r}\right)^n, & r > R, \quad T_1 \le z \le h, \\ 0, & 0 \le z < T_1. \end{cases} \tag{68}$$

This specification includes the previous example of unbounded solid-body rotation ($n = -1$) and the classical Rankine vortex ($n = 1$). For $n > 1$, the vertical vorticity in the outer region is negative. In the following, we restrict attention to $n > 0$ to ensure that the azimuthal velocity decays with radius.

TABLE 1. Parameter settings for selected three-layer vortices with $\tilde{T}_1(0) = \tilde{T}_2(0) = 1/3$. Vortex names consist of a letter followed by the ratio $\varphi_1(0)/\varphi_2(0)/\varphi_3(0)$ of initial layer angular velocities. All quantities are nondimensional.

Vortex	$\varphi_1(0)/\overline{\varphi}$	$\varphi_2(0)/\overline{\varphi}$	$\varphi_3(0)/\overline{\varphi}$	$P(0)$	$Q(0)$	α	β	γ
A1:2:4	0.5833	1.1666	2.3333	0.0	0.0	6.125	24.500	98.000
B1:2:10	0.5333	1.0666	5.3333	0.0	0.0	5.120	20.480	512.00
C1:2:4	0.5833	1.1666	2.3333	0.0	−0.5	6.125	24.500	98.000
D1:2:10	0.5333	1.0666	5.3333	0.0	−0.5	5.120	20.480	512.00

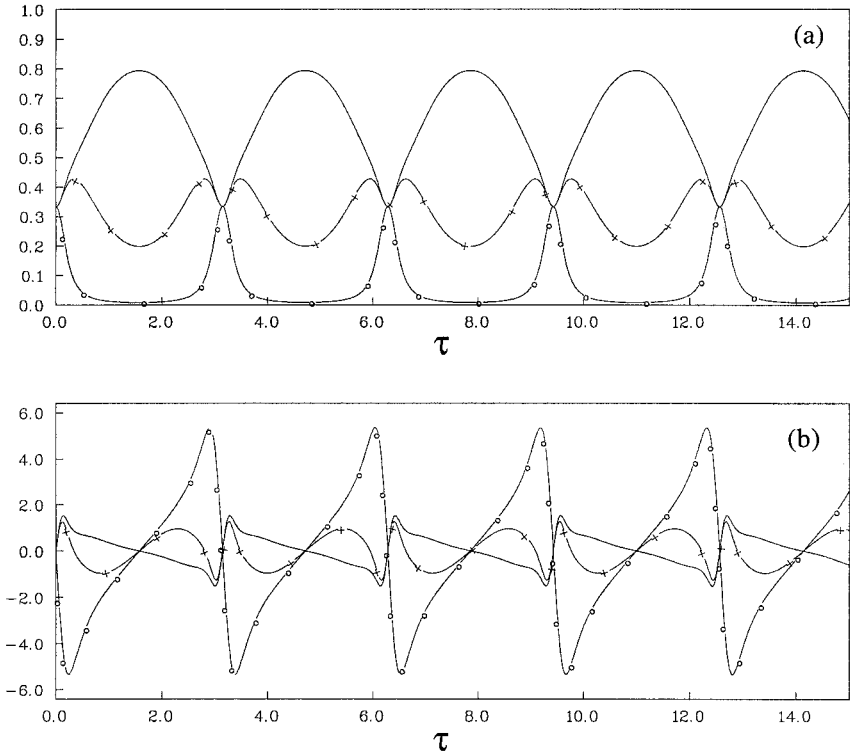

FIG. 5. As in Fig. 4 but for vortex B1:2:10, a three-layer vortex with initial layer angular velocities increasing upward in a ratio of 1:2:10.

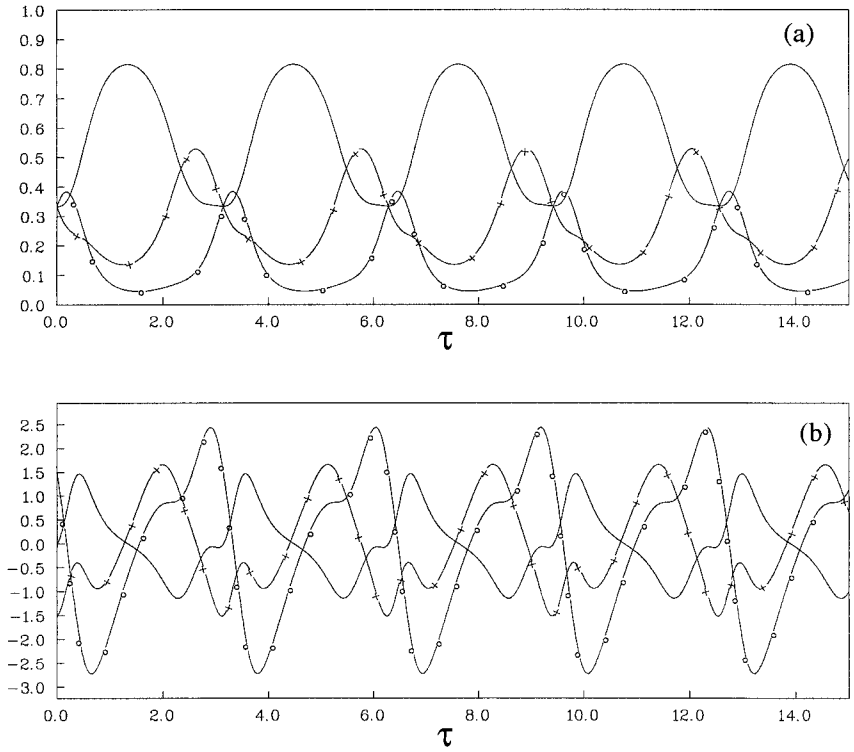

FIG. 6. As in Fig. 4 but for vortex C1:2:4, a three-layer vortex with an upper interface initially descending with $Q(0) = -0.5$.

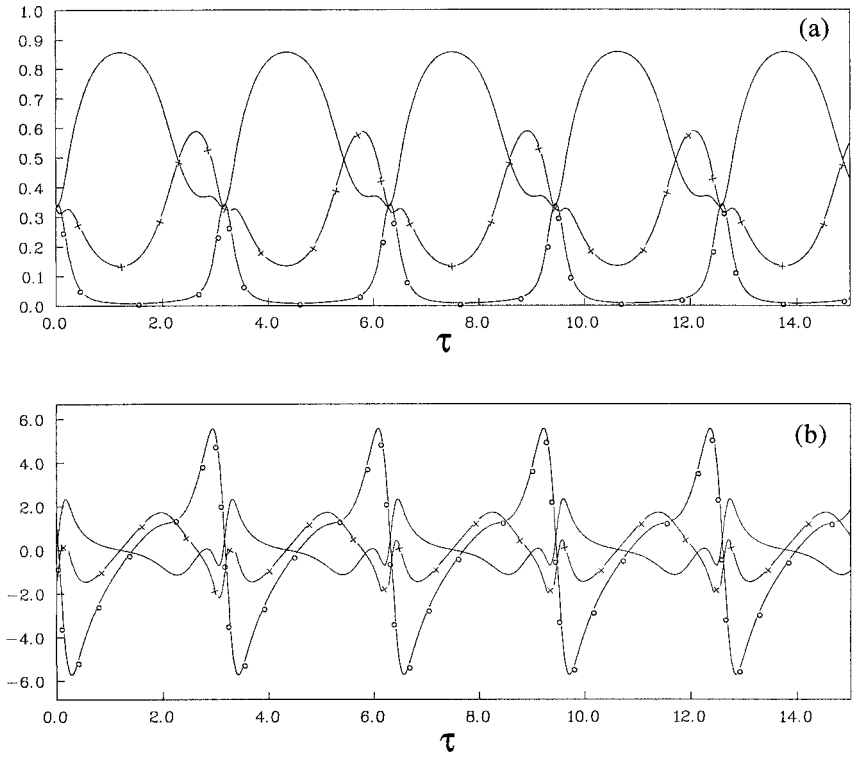

FIG. 7. As in Fig. 4 but for vortex D1:2:10, a three-layer vortex with initial layer angular velocities increasing upward in a ratio of 1:2:10, and with an upper interface initially descending with $Q(0) = -0.5$.

In the absence of an initial secondary circulation, the azimuthal equation of motion (2) shows that the initial azimuthal velocity tendency is zero, while the azimuthal vorticity equation (12) yields an equation for the initial streamfunction tendency ψ^1 [$\equiv \partial\psi/\partial t(r, z, 0)$],

$$\frac{\partial^2\psi^1}{\partial z^2} + \frac{\partial^2\psi^1}{\partial r^2} - \frac{1}{r}\frac{\partial\psi^1}{\partial r} = \frac{\partial v^{0^2}}{\partial z}. \tag{69}$$

The right-hand side of (69) vanishes everywhere except along the interfacial singularity at $z = T_1$. Integrating (69) an infinitesimal distance across this discontinuity, we obtain a jump condition for $\partial\psi^1/\partial z$ (indicating a jump in the radial velocity tendency and thus a jump in the radial velocity itself),

$$\frac{\partial\psi^1}{\partial z}(r, T_1^+) - \frac{\partial\psi^1}{\partial z}(r, T_1^-) = v^{0^2}(r, T_1^+), \tag{70}$$

where $T_1^+ \equiv \lim_{|\varepsilon|\to 0}(T_1 + |\varepsilon|)$ and $T_1^- \equiv \lim_{|\varepsilon|\to 0}(T_1 - |\varepsilon|)$. We take ψ^1 itself as being continuous across the interface so that the normal velocity component is continuous.

Thus, we seek solutions of

$$\frac{\partial^2\psi^1}{\partial z^2} + \frac{\partial^2\psi^1}{\partial r^2} - \frac{1}{r}\frac{\partial\psi^1}{\partial r} = 0, \tag{71}$$

satisfying the jump condition (70) at $z = T_1$. We impose the impermeability condition on the top and bottom boundaries, assume there is no source or sink of mass along the axis of symmetry, and let the mass flux vanish far from the axis of symmetry,

$$\psi^1(0, z) = \psi^1(r, 0) = \psi^1(r, h) = \psi^1(\infty, z) = 0. \tag{72}$$

Solving (70)–(72) for ψ^1 (see the appendix), we obtain

$$\psi^1 = \sum_{k=1}^{\infty} \frac{2\Omega^2R^2h}{k^2\pi^2}F(r)\sin\left(\frac{k\pi T_1}{h}\right)\sin\left(\frac{k\pi z}{h}\right), \tag{73}$$

where

$$\begin{aligned} F(r) = {} & -4n(n+1)\frac{r}{R}I_1\left(\frac{k\pi r}{h}\right)\int_1^{\infty}\frac{K_1(k\pi xR/h)}{x^{2n+2}}\,dx - \frac{r^2}{R^2} \\ & + 2(n+1)\frac{r}{R}I_1\left(\frac{k\pi r}{h}\right)K_1\left(\frac{k\pi R}{h}\right), \qquad r < R, \\ = {} & 2(n+1)\frac{r}{R}K_1\left(\frac{k\pi r}{h}\right)I_1\left(\frac{k\pi R}{h}\right) \\ & - 4n(n+1)\frac{r}{R}K_1\left(\frac{k\pi r}{h}\right)\int_1^{r/R}\frac{I_1(k\pi xR/h)}{x^{2n+2}}\,dx \\ & - 4n(n+1)\frac{r}{R}I_1\left(\frac{k\pi r}{h}\right)\int_{r/R}^{\infty}\frac{K_1(k\pi xR/h)}{x^{2n+2}}\,dx \end{aligned}$$

$$-\left(\frac{R}{r}\right)^{2n}. \qquad r > R \tag{74}$$

This solution was evaluated for a range of aspect ratios R/h, decay exponents n, and interface heights T_1. The modified Bessel functions I_1 and K_1 were evaluated with the IMSL MATH/LIBRARY special functions FORTRAN subroutines BSI1 and BSK1, respectively, except for large arguments (>10), where asymptotic formulas were used (Abramowitz and Stegun 1964). The integrals were evaluated with the trapezoidal rule. Although analytic forms for the initial meridional velocity tendencies u^1 [$\equiv(1/r)\partial\psi^1/\partial z$] and w^1 [$\equiv(-1/r)\partial\psi^1/\partial r$] are available, it is convenient to obtain these components from ψ^1 via finite-difference discretizations.

Results are presented for vortices overlying nonrotating fluid of depth $T_1 = 0.2h$. We consider a columnar vortex ($R/h = 0.5$) with weak ($n = 1$) and strong ($n = 4$) outer decay (Figs. 8 and 9, respectively), and a broad vortex ($R/h = 2$) with weak ($n = 1$) and strong ($n = 4$) outer decay (Figs. 10 and 11, respectively). In all cases an updraft extends across the vortex core as well as in the nonrotating flow beneath the core. The peak updraft speed at a fixed radius occurs at the horizonal interface between the rotating and nonrotating fluid. The updraft strength and pattern (i.e., flatness of vertical velocity isolines) is remarkably similar for vortices of the same aspect ratio, with greater flatness for the broader vortices.

The near constancy of w with respect to radius in the core region and the relative insensitivity of the updraft to the decay exponent suggest that the similarity solutions presented in the previous sections may be applicable within the core region of the finite radius vortices, at least for a short time. This can be seen for the examples considered herein by comparing Figs. 8–11 with Fig. 12. This latter figure depicts the azimuthal velocity and the time tendency of the meridional velocity fields for a radially unbounded (similarity) vortex overlying nonrotating fluid (initial depth of $0.2h$). Direct comparison with the linear finite radius solutions is facilitated by evaluating the similarity solution (55) at a small nondimensional time $\Omega t = 0.247\,48$ (when the interface has risen slightly to $0.21h$), expressing the meridional velocity fields as tendencies (u/t and w/t, at small time t) and contouring the scaled fields to match Figs. 8–11. As can be seen, the similarity solution is in good quantitative agreement with the broad linear vortices (Figs. 10 and 11) for radii extending to ~¾ of the core radius. In contrast, the similarity solution exhibits only good qualitative agreement with the two columnar vortices, and then only out to ~½ the core radius. For radii near and beyond the core radius, the similarity solution departs significantly from both the broad and columnar vortices. Since the similarity solution is independent of a radial length scale, it is not surprising that it is in better agreement with the broader vortices than the columnar vortices. Indeed, it can be shown that for an infinite aspect ratio R/h, the vertical velocity tendency associated with the linear solution (73) reduces to the vertical velocity tendency associated with the nonlinear similarity solution (55) in the limit of vanishing time.

Perhaps the most intriguing feature in Figs. 8–11 is the annular downdraft ringing the updraft just beyond the radius of maximum tangential wind. This downdraft is very sensitive to the aspect ratio and decay exponent, being stronger and narrower for larger R/h and larger n. Indeed, for the broad vortex with strong radial decay depicted in Fig. 11, the peak downdraft speed actually exceeds the peak updraft speed. Although our linear analysis should not be used to quantify the angular momentum transport in this downdraft, qualitatively we see that the downdraft is at least ''poised'' to transport vortex angular momentum downward and radially inward. A complete picture of angular momentum transport in the downdraft and its subsequent feedback on the secondary circulation must await a nonlinear numerical simulation. Of course, whether these symmetric vortex-induced downdrafts are physically realizable depends, in part, on the stability of the solutions. Of particular interest is the stability of these vortices with anticyclonic vorticity in the outer region, that is, when Rayleigh's stability criterion is violated. Determining the stability bounds of our unsteady vortices, while important, is a formidable task and must be deferred to a future study.

7. Summary and discussion

This investigation is concerned with the inviscid dynamics of vortices with axially varying rotation rates, including the case of a vortex overlying nonrotating fluid. We consider radially unbounded vortices in solid body rotation and elevated Rankine-type vortices. For the former class of vortices, the von Kármán–Bödewadt similarity principle is applicable and leads to exact unsteady solutions of the nonlinear Euler equations. These similarity solutions are noteworthy in that the meridional circulation is not prescribed but is generated by the vortex circulation. The solutions describe decaying, amplifying, and oscillatory behavior for both the primary vortex and the vortex-induced secondary circulation.

The behavior of the oscillatory similarity solutions is typified by the case of a strong vortex overlying a weaker vortex. In this case the radial pressure gradient force induces a converging low-level flow and an associated updraft that spins up the initially weak lower-layer vorticity to values exceeding that in the upper-layer vortex. The reversed axial distribution of vorticity (and the associated reversal of the axial pressure gradient force) causes a reversal of the secondary circulation with a subsequent spindown of the low-level vorticity. For our inviscid, unforced hydrodynamical model, the oscillation proceeds ad infinitum.

The absence of a radial length scale and the unbounded nature of the similarity scalings (u and v increase

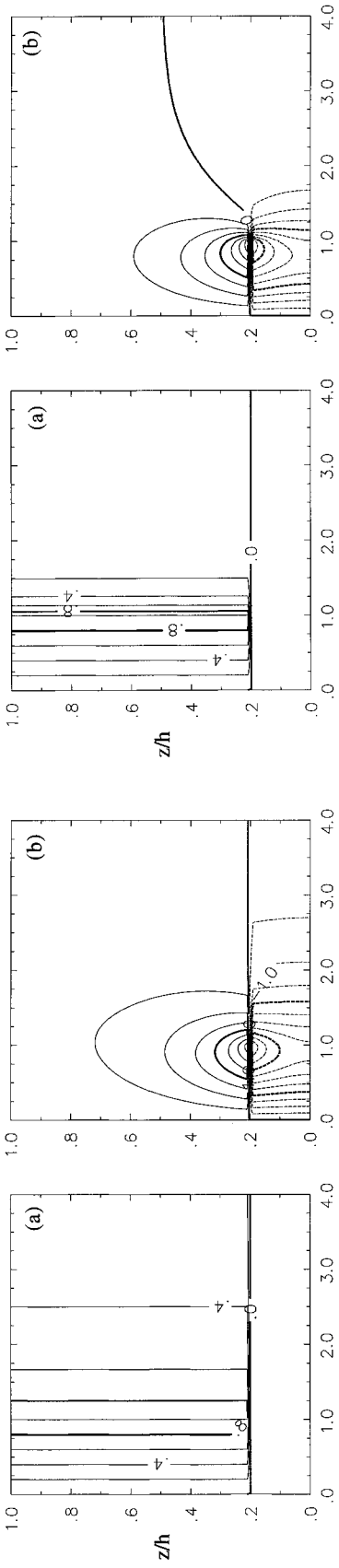

FIG. 8. Initial azimuthal velocity and initial tendency fields for a columnar vortex with weak radial decay ($R/h = 0.5$, $n = 1$). Low-level nonrotating fluid depth is $T_1 = 0.2h$. (a) Azimuthal velocity $v^0/(\Omega R)$, (b) radial velocity tendency $u^1 \times 10/(R\Omega^2)$, (c) streamfunction tendency $\psi^1 \times 10/(h\Omega^2 R^2)$, and (d) vertical velocity tendency $w^1 \times 10/(h\Omega^2)$. Negative contours in (b) and (d) are dashed.

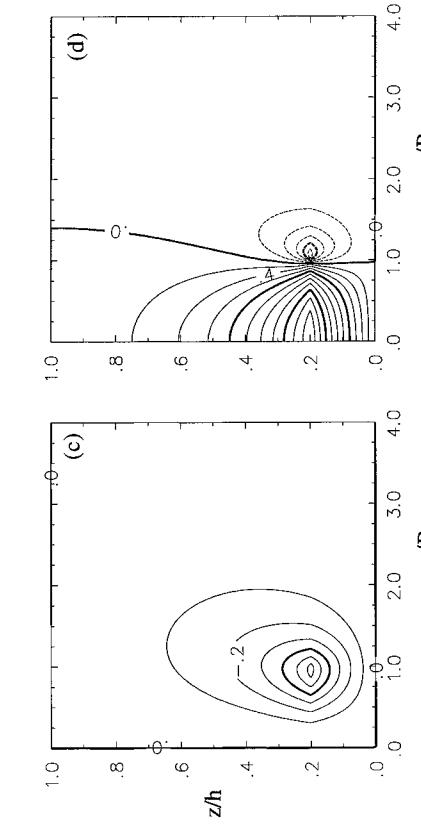

FIG. 9. As in Fig. 8 but for a columnar vortex with strong radial decay ($R/h = 0.5$, $n = 4$).

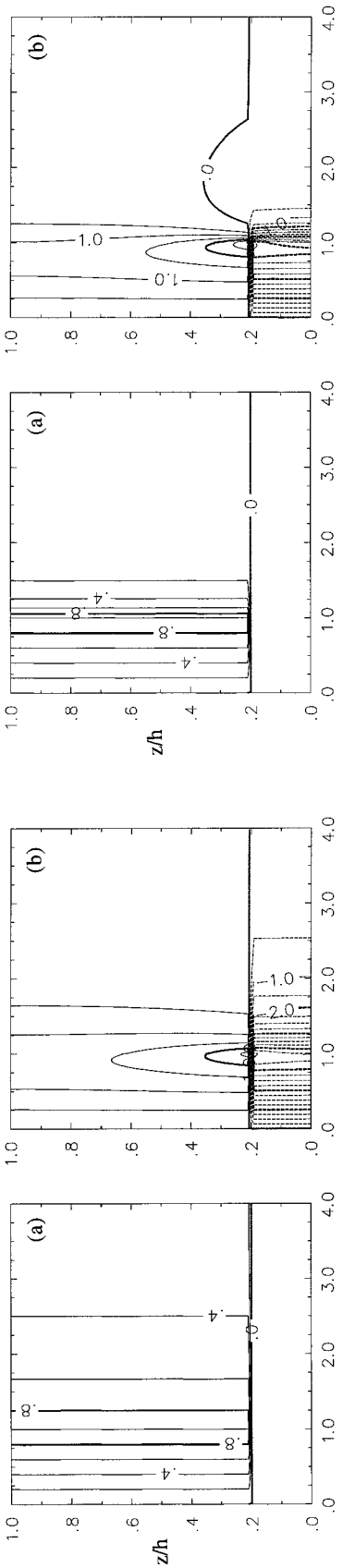

FIG. 10. As in Fig. 8 but for a broad vortex with weak radial decay ($R/h = 2$, $n = 1$).

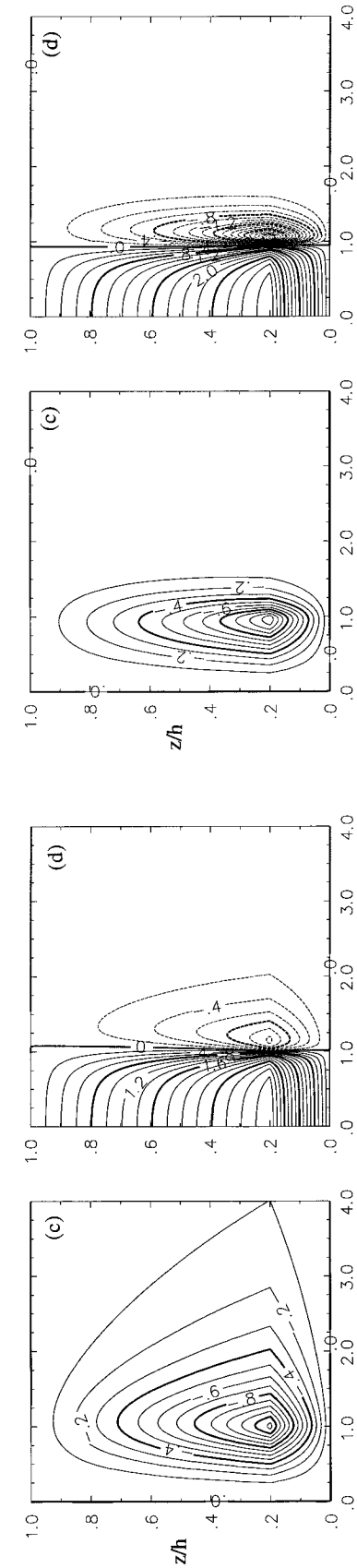

FIG. 11. As in Fig. 8 but for a broad vortex with strong radial decay ($R/h = 2$, $n = 4$).

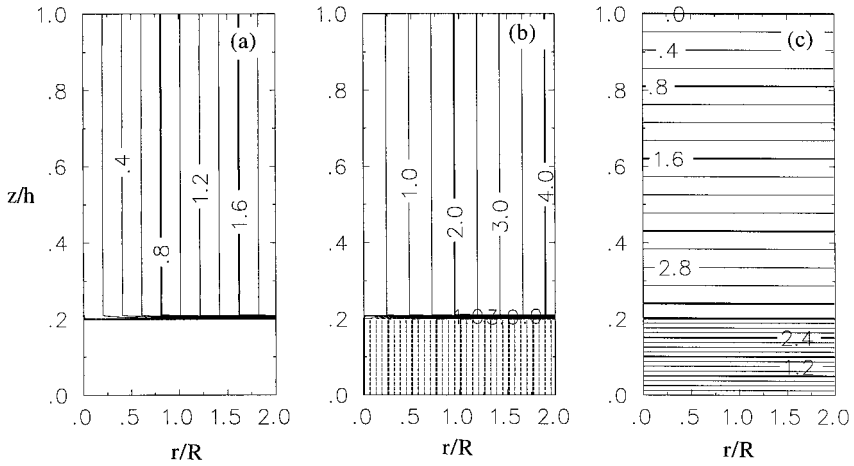

FIG. 12. Similarity solution for a radially unbounded vortex overlying nonrotating fluid with initial depth of 0.2h. Fields are obtained from (55) at nondimensional time $\Omega t = 0.247\,48$, that is, when the interface has risen slightly to 0.21h. (a) Azimuthal velocity $v/(\Omega R)$, (b) radial velocity tendency $u/t \times 10/(R\Omega^2)$, and (c) vertical velocity tendency $w/t \times 10/(h\Omega^2)$. Negative contours in (b) are dashed. Fields are scaled in the same manner and plotted with the same contour interval as in Figs. (8)–(11).

with radius, while w and $\partial p/\partial z$ are independent of radius) suggest that the similarity solutions may be most relevant to the dynamics of the interior portions of broad mesoscale vortices. The dynamics embodied by the similarity solutions might also be important as a modulating factor for columnar vortices embedded within a broader parent vortex. A comparison (at a small time) between a similarity solution and its finite radius counterpart in section 6 indicated that the similarity solution was in better agreement with the broader vortices than the columnar vortices. However, long time numerical simulations of a variety of finite radius vortices will be required to establish the areal and temporal bounds of validity of the similarity solutions.

The oscillatory behavior of the similarity solutions appears to be similar to the vortex valve effect sometimes used to explain the cyclic appearance, demise, and reappearance of supercell characteristics in tornadic storms and the apparent paradox of tornado formation in association with storm top collapse (Lemon et al. 1975; Davies-Jones 1986). The vortex valve effect can be demonstrated in a vortex chamber by feeding low-level rotating air into an updraft that vents through a hole at the top of the chamber. As the rotating air approaches the axis of symmetry at low levels, the azimuthal velocity increases in accordance with angular momentum conservation. The increased low-level azimuthal velocity is associated with a decrease in low-level pressure, a reduction of the upward axial pressure gradient force, and a ''choking'' of the updraft. Most columnar geophysical vortices with axially varying rotation rates will not have the radial pressure gradient independent of the axial direction. However, we believe the essential dynamical mechanism for real vortex–updraft oscillations is provided in its most basic form by our similarity model.

We also examine the short-term behavior of elevated vortices with cores in solid body rotation embedded within radially decaying angular momentum profiles, a class that includes the elevated Rankine vortex. A linear analysis of this case shows that an annular downdraft should form on the periphery of the vortex core. The peak vortex-induced downdraft speed is greatest for broad vortex cores and for large outer vortex radial-decay rates, and can exceed the peak vortex-induced updraft speed. Although our linear analysis should not be used to quantify angular momentum transport, based on the form of the downdraft we hypothesize that the vortex angular momentum can be advected downward and radially inward. The details of this transport and its subsequent feedback on the meridional circulation are of particular interest. For what set of parameters does the angular momentum remain suspended or reach the ground? For what set of parameters does the radial convergence cause the angular momentum to spin up at midlevels and build downward via the dynamic pipe effect (Smith and Leslie 1978; Trapp and Davies-Jones 1997) or first descend to the ground, spin up in the converging low-level flow and then build upward? Is an oscillation set up, as in the similarity solutions? Clearly a longer-term nonlinear simulation is required to answer these questions.

It should be borne in mind that our hydrodynamical model of elevated rotation of finite radius with no initial meridional circulation is highly specialized. This model was chosen because it provided one of the simplest possible ''thought experiments'' for studying the behavior of elevated vortices. Evidence for a dynamically in-

duced downdraft in real mesocyclones or other geophysical vortices will require careful analysis of high resolution four-dimensional data from observed or numerically modeled phenomena. We note that in Fig. 9d of Ray et al. (1981) an ''unexplained'' elongated downdraft appears in the multiple-Doppler analysis of the Del City storm at $z = 2$ km ''. . . in inflow air characterized by weak reflectivities. . . .'' This narrow north–south-oriented downdraft straddles a line extending from approximately $x = 5$, $y = 8$ to $x = 5$, $y = 15$. It appears along the edge of the mesocyclone at the approximate location of the maximum wind, and may be a manifestation of the vortex-induced downdraft discussed herein [Figs. 9e and 9f of Ray et al. (1981) also show a downdraft ringing much of the mesocyclone at the 2-km level, though much of this is likely associated with precipitation loading]. Brooks et al. (1993) found a downdraft in a similar position, but attributed it to the presence of an inflow low due to high wind speeds at low levels (Bernoulli relationship). We also note the fortuitous measurements of a dust devil that struck an instrumented tower while data acquisition was in progress (Kaimal and Businger 1970). Measurements of the horizontal and vertical velocity components were taken at heights of 5.66 and 22.6 m. The trace of the lower-level data revealed a narrow downdraft on either side of the dust devil updraft in the zone of radially decreasing tangential velocity (Fig. 2 of Kaimal and Businger 1970).

Downdrafts, though not necessarily annular downdrafts, have been implicated in mesocyclonic tornadogenesis. Davies-Jones (1982a,b) argued that tilting and stretching of environmental horizontal vorticity by an updraft alone would fail to produce appreciable rotation at low levels (i.e., only a midlevel mesocyclone would be produced), since vertical vorticity is generated only as parcels move upward, away from the ground, in an updraft. This was verified in the numerical simulations of Rotunno and Klemp (1985). Davies-Jones hypothesized that a downdraft was necessary for the genesis of near-ground rotation.

Barnes (1978) and Lemon and Doswell (1979) hypothesized that the transition to tornadic phase in a supercell is initiated by the rear-flank downdraft (RFD). They suggested that the RFD formed at midlevels and intensified the low-level rotation by creating strong shear (Barnes) or thermal gradients (Lemon and Doswell) between the updraft and the RFD. Browning and Donaldson (1963) may have provided the first documentation of the RFD in an early supercell study.

Three-dimensional numerical simulations (Klemp and Rotunno 1983) have, however, implied the opposite cause and effect relationship; the low-level rotation intensifies, followed by formation of an ''occlusion downdraft,'' a smaller-scale downdraft within the RFD. In this scenario, Klemp and Rotunno hypothesized that the RFD is dynamically driven by a local, low-level pressure drop due to the intensifying rotation, which generates a downward-directed pressure gradient. Brandes (1984a,b) also presented this hypothesis based on Doppler radar analysis. Our proposed mechanism of downdraft formation and downward transport of angular momentum relies on the presence of strong elevated rotation and thus differs from Rotunno and Klemp's (1983) occlusion downdraft, which is driven by strong low-level rotation. The reader is referred to Klemp (1987) and Davies-Jones and Brooks (1993) for more detailed surveys of past modeling and theoretical studies.

We hypothesize that the hydrodynamic vortex-induced process described herein may play a role in lower-level mesocyclogenesis or tornadogenesis, either through the formation of an annular (or semiannular) downdraft or by facilitating the development of an RFD. This basic process may be important in vortex-dominated flows in other geophysical and engineering contexts as well. The longer-term behavior of our idealized vortex including the downward transport of the vortex circulation by the annular downdraft will be examined in future numerical simulations.

Acknowledgments. Detailed and insightful comments by the anonymous referees led to a substantially improved manuscript. Discussions with Doug Lilly and Kathy Kanak are gratefully acknowledged. Tom Condo, Tim Kwiatkowski, and Courtney Garrison provided computer assistance. This research was supported by the Center for Analysis and Prediction of Storms (CAPS) under Grant ATM91-20009 from the National Science Foundation. One of us (P.M.) was supported by an AMS fellowship sponsored by GTE Federal Systems Division, Chantilly, Virginia.

APPENDIX

Derivation of the Initial Streamfunction Tendency ψ^1

We seek the initial streamfunction tendency ψ^1 satisfying the partial differential equation (71), the jump condition (70), and the boundary conditions (72). Toward that end, introduce a function Ψ satisfying (70) and (72),

$$\begin{aligned} \Psi &= -g(z)\Omega^2 r^2, && r < R, \\ &= -g(z)\Omega^2 R^2 \left(\frac{R}{r}\right)^{2n}, && r > R, \end{aligned} \tag{A1}$$

where

$$\begin{aligned} g(z) &= \left(1 - \frac{T_1}{h}\right) z, && 0 \le z < T_1, \\ &= \frac{T_1}{h}(h - z), && T_1 < z \le h. \end{aligned} \tag{A2}$$

For later use we note that $g(z)$ can be extended as an odd periodic function of period $2h$,

$$g(z) = \sum_{k=1}^{\infty} \frac{2h}{k^2\pi^2} \sin\left(\frac{k\pi T_1}{h}\right) \sin\left(\frac{k\pi z}{h}\right), \quad 0 \le z \le h. \tag{A3}$$

Although Ψ does not satisfy (71), ψ^1 $(=\Psi + \Phi)$ does satisfy (71) provided that Φ satisfies

$$\frac{\partial^2\Phi}{\partial z^2} + \frac{\partial^2\Phi}{\partial r^2} - \frac{1}{r}\frac{\partial\Phi}{\partial r} = 4n(n+1)g(z)\Omega^2\left(\frac{R}{r}\right)^{2n+2}, \quad r > R, \qquad = 0, \quad r < R. \tag{A4}$$

In terms of Φ, the boundary conditions (72) become

$$\Phi(0, z) = \Phi(r, 0) = \Phi(r, h) = \Phi(\infty, z) = 0. \tag{A5}$$

We also want to ensure that the full solution $\Psi + \Phi$ and its normal derivative $\partial\Psi/\partial r + \partial\Phi/\partial r$ are continuous at $r = R$. Since $\partial\Psi/\partial r$ obtained from (A1) is discontinuous at $r = R$, there must be an equal and opposite discontinuity in $\partial\Phi/\partial r$,

$$\frac{\partial\Phi}{\partial r}(R^+, z) - \frac{\partial\Phi}{\partial r}(R^-, z) = -2(n+1)g(z)\Omega^2 R, \tag{A6}$$

where $R^+ \equiv \lim_{|\varepsilon|\to 0}(R + |\varepsilon|)$, and $R^- \equiv \lim_{|\varepsilon|\to 0}(R - |\varepsilon|)$.

Applying (A3) in (A4), and expanding Φ in a sine series, we obtain

$$\Phi = \sum_{k=1}^{\infty} \frac{8n(n+1)\Omega^2 h}{k^2\pi^2} f_k(r) \sin\left(\frac{k\pi T_1}{h}\right) \sin\left(\frac{k\pi z}{h}\right), \tag{A7}$$

where $f_k(r)$ satisfies

$$\frac{\partial^2 f_k}{\partial r^2} - \frac{1}{r}\frac{\partial f_k}{\partial r} - \frac{k^2\pi^2}{h^2} f_k = \left(\frac{R}{r}\right)^{2n+2}, \quad r > R, \qquad = 0, \quad r < R. \tag{A8}$$

Applying (A3) and (A7) in (A6), we obtain the radial jump condition,

$$\frac{df_k}{dr}(R^+) - \frac{df_k}{dr}(R^-) = -\frac{R}{2n}. \tag{A9}$$

The solution of (A8) in the core region is

$$f_k = c_1 r I_1\left(\frac{k\pi r}{h}\right), \quad r < R, \tag{A10}$$

where I_1 is a modified Bessel function of the first kind of order one and c_1 is a constant. The second linearly dependent solution, a modified Bessel function of the third kind of order one, K_1, was rejected because of its singular behavior at the origin. Recurrence relations, derivative formulas, and other results pertaining to modified Bessel functions are described in Abramowitz and Stegun (1964) and Watson (1944).

The solution of (A8) in the outer region can be expressed in terms of Lommel's functions [section 10.7 of Watson (1944)], or left in a form obtained by the method of variation of parameters,

$$f_k = -RrK_1\left(\frac{k\pi r}{h}\right)\int_1^{r/R} \frac{I_1(k\pi xR/h)}{x^{2n+2}}\,dx - RrI_1\left(\frac{k\pi r}{h}\right)\int_{r/R}^{\infty} \frac{K_1(k\pi xR/h)}{x^{2n+2}}\,dx + c_2 rK_1(k\pi r/h), \quad r > R. \tag{A11}$$

Here one of the two constants in the general solution was specified to make f_k vanish at infinity. To verify this behavior, write f_k as a sum of indeterminate forms, apply L'Hôpital's rule, and use asymptotic and derivative formulas for modified Bessel functions:

$$\lim_{r\to\infty} f_k = -R\lim_{r\to\infty}\left[\frac{\int_1^{r/R} \frac{I_1(k\pi xR/h)}{x^{2n+2}}\,dx}{1/[rK_1(k\pi r/h)]} + \frac{\int_{r/R}^{\infty} \frac{K_1(k\pi xR/h)}{x^{2n+2}}\,dx}{1/[rI_1(k\pi r/h)]}\right] = -\lim_{r\to\infty}\frac{h^2}{k^2\pi^2}\left(\frac{R}{r}\right)^{2n+2}.$$

Thus f_k vanishes at infinity for the cases of interest, $n > 0$. Moreover, since Φ decays by a factor of $1/r^2$ faster than Ψ, the solution $\psi^1 = \Psi + \Phi$ is dominated by Ψ far from the axis of symmetry.

Continuity of f_k at $r = R$ and the radial jump condition (A9) yield two equations for c_1 and c_2,

$$c_1 RI_1\left(\frac{k\pi R}{h}\right) = c_2 RK_1\left(\frac{k\pi R}{h}\right) - R^2 I_1\left(\frac{k\pi R}{h}\right)\int_1^{\infty} \frac{K_1(k\pi xR/h)}{x^{2n+2}}\,dx, \tag{A12}$$

$$-R^2 I_0\left(\frac{k\pi R}{h}\right)\int_1^{\infty} \frac{K_1(k\pi xR/h)}{x^{2n+2}}\,dx - c_2 RK_0\left(\frac{k\pi R}{h}\right) - c_1 RI_0\left(\frac{k\pi R}{h}\right) = -\frac{Rh}{2k\pi n}. \tag{A13}$$

Solving (A12) and (A13) and applying a formula for the Wronskian of Bessel functions, we get

$$c_1 = -R \int_1^{\infty} \frac{K_1(k\pi xR/h)}{x^{2n+2}}\, dx + \frac{R}{2n} K_1\left(\frac{k\pi R}{h}\right), \quad \text{(A14)}$$

$$c_2 = \frac{R}{2n} I_1\left(\frac{k\pi R}{h}\right). \quad \text{(A15)}$$

This completes the specification of the initial streamfunction tendency. Collecting results, we write the solution as (73) and (74).

REFERENCES

Abramowitz, M., and I. A. Stegun, 1964: *Handbook of Mathematical Functions with Formulas, Graphs, and Mathematical Tables.* National Bureau of Standards, 1046 pp.

Aref, H., N. Rott, and H. Thomann, 1992: Grobli's solution of the three-vortex problem. *Annu. Rev. Fluid Mech.,* **24,** 1–20.

Ball, F. K., 1963: Some general theorems concerning the finite motion of a shallow liquid lying on a paraboloid. *J. Fluid Mech.,* **17,** 240–256.

——, 1964: An exact theory of simple finite shallow water oscillations on a rotating earth. *Hydraulics and Fluid Mechanics,* R. Silvester, Ed., Macmillan, 293–305.

——, 1965: The effect of rotation on the simpler modes of motion of a liquid in an elliptic paraboloid. *J. Fluid Mech.,* **22,** 529–545.

Barnes, S. L., 1978: Oklahoma thunderstorms on 29–30 April 1970. Part I: Morphology of a tornadic storm. *Mon. Wea. Rev.,* **106,** 673–684.

Batchelor, G. K., 1951: Note on a class of solutions of the Navier–Stokes equations representing steady rotationally-symmetric flow. *Quart. J. Mech. Appl. Math.,* **4,** 29–41.

——, 1967: *An Introduction to Fluid Dynamics.* Cambridge University Press, 615 pp.

Bellamy-Knights, P. G., 1970: An unsteady two-cell vortex solution of the Navier–Stokes equations. *J. Fluid Mech.,* **41,** 673–687.

——, 1971: Unsteady multicellular viscous vortices. *J. Fluid Mech.,* **50,** 1–16.

——, and R. Saci, 1983: Unsteady convective atmospheric vortices. *Bound.-Layer Meteor.,* **27,** 371–386.

Bödewadt, U. T., 1940: Die Drehströmung über festem Grunde. *Z. angew. Math. Mech.,* **20,** 241–253.

Bodonyi, R. J., 1978: On the unsteady similarity equations for the flow above a rotating disc in a rotating fluid. *Quart. J. Mech. Appl. Math.,* **31,** 461–472.

——, and K. Stewartson, 1977: The unsteady laminar boundary layer on a rotating disk in a counter-rotating fluid. *J. Fluid Mech.,* **79,** 669–688.

Bragg, S. L., and W. R. Hawthorne, 1950: Some exact solutions of the flow through annular cascade actuator discs. *J. Aeronaut. Sci.,* **17,** 243–249.

Brandes, E. A., 1984a: Relationships between radar-derived thermodynamic variables and tornadogenesis. *Mon. Wea. Rev.,* **112,** 1033–1052.

——, 1984b: Vertical vorticity generation and mesocyclone sustenance in tornadic thunderstorms: The observational evidence. *Mon. Wea. Rev.,* **112,** 2253–2269.

——, R. P. Davies-Jones, and B. C. Johnson, 1988: Streamwise vorticity effects on supercell morphology and persistence. *J. Atmos. Sci.,* **45,** 947–963.

Brooks, H. E., C. A. Doswell III, and R. P. Davies-Jones, 1993: Environmental helicity and the maintenance and evolution of low-level mesocyclones. *The Tornado: Its Structure, Dynamics, Prediction, and Hazards, Geophys. Monogr.,* No. 79, Amer. Geophys. Union, 97–104.

Browning, K. A., and R. J. Donaldson Jr., 1963: Airflow and structure of a tornadic storm. *J. Atmos. Sci.,* **20,** 533–545.

Burgers, J. M., 1948: A mathematical model illustrating the theory of turbulence. *Adv. Appl. Mech.,* **1,** 171–199.

Cushman-Roisin, B., 1984: An exact analytical solution for a time-dependent, elliptical warm-core ring with outcropping interface. *Ocean Modelling,* **59,** 5–6.

——, 1987: Exact analytical solutions for elliptical vortices of the shallow-water equations. *Tellus,* **39A,** 235–244.

——, W. H. Heil, and D. Nof, 1985: Oscillations and rotations of elliptical warm-core rings. *J. Geophys. Res.,* **90,** 11 756–11 764.

Davies-Jones, R. P., 1982a: Observational and theoretical aspects of tornadogenesis. *Topics in Atmospheric and Oceanic Sciences: Intense Atmospheric Vortices,* L. Bengtsson and J. Lighthill, Eds., Springer-Verlag, 175–189.

——, 1982b: A new look at the vorticity equation with application to tornadogenesis. Preprints, *12th Conf. on Severe Local Storms,* Boston, MA, Amer. Meteor. Soc., 249–252.

——, 1985: Dynamical interaction between an isolated convective cell and a veering environmental wind. Preprints, *14th Conf. on Severe Local Storms,* Indianapolis, IN, Amer. Meteor. Soc., 216–219.

——, 1986: Tornado dynamics. *Thunderstorm Morphology and Dynamics,* 2d ed., Univeristy of Oklahoma Press, 197–236.

——, and H. Brooks, 1993: Mesocyclogenesis from a theoretical perspective. *The Tornado: Its Structure, Dynamics, Prediction, and Hazards, Geophys. Monogr.,* No. 79, Amer. Geophys. Union, 105–114.

Greenspan, H. P., 1968: *The Theory of Rotating Fluids.* Cambridge University Press, 327 pp.

Gutman, L. N. 1957: Theoretical model of a waterspout. *Bulletin of the Academy of Science USSR.* Geophysics Series, Vol. 1, Pergamon Press translation, 87–103.

Hatton, L., 1975: Stagnation point flow in a vortex core. *Tellus,* **27,** 269–280.

Hill, M. J. M., 1894: On a spherical vortex. *Philos. Trans. Roy. Soc. London, Ser. A,* **185,** 213–245.

Kaimal, J. C., and J. A. Businger, 1970: Case studies of a convective plume and a dust devil. *J. Appl. Meteor.,* **9,** 612–620.

Klemp, J. B., 1987: Dynamics of tornadic thunderstorms. *Ann. Rev. Fluid Mech.,* **19,** 369–402.

——, and R. Rotunno, 1983: A study of the tornadic region within a supercell thunderstorm. *J. Atmos. Sci.,* **40,** 359–377.

Kuo, H. L., 1966: On the dynamics of convective atmospheric vortices. *J. Atmos. Sci.,* **23,** 25–42.

——, 1967: Note on the similarity solutions of the vortex equations in an unstably stratified atmosphere. *J. Atmos. Sci.,* **24,** 95–97.

Lamb, H., 1945: *Hydrodynamics.* Dover Publications, 738 pp.

Lemon, L. R., and C. A. Doswell III, 1979: Severe thunderstorm evolution and mesocyclone structure as related to tornadogenesis. *Mon. Wea. Rev.,* **107,** 1184–1197.

——, D. W. Burgess, and R. A. Brown, 1975: Tornado production and storm sustenance. Preprints, *Ninth Conf. on Severe Local Storms,* Norman, OK, Amer. Meteor. Soc., 100–104.

Lewellen, W. S., 1993: Tornado vortex theory. *The Tornado: Its Structure, Dynamics, Prediction and Hazards, Geophys. Monogr.,* No. 79, Amer. Geophys. Union, 19–39.

Lilly, D. K., 1983: Dynamics of rotating thunderstorms. *Mesoscale Meteorology—Theories, Observations, and Models,* D. K. Lilly and T. Gal-Chen, Eds., D. Reidel, 531–544.

——, 1986: The structure, energetics and propagation of rotating convective storms. Part II: Helicity and storm stabilization. *J. Atmos. Sci.,* **43,** 126–140.

Long, R. R., 1956: Sources and sinks at the axis of a rotating liquid. *Quart. J. Mech. Appl. Math.,* **9,** 385–393.

——, 1958: Vortex motion in a viscous fluid. *J. Meteor.,* **15,** 108–112.

——, 1961: A vortex in an infinite viscous fluid. *J. Fluid Mech.,* **11,** 611–624.

Lugt, H. J., 1983: *Vortex Flow in Nature and Technology.* John Wiley and Sons, 297 pp.

Miles, J. W., and F. K. Ball, 1963: On free-surface oscillations in a rotating paraboloid. *J. Fluid Mech.,* **17,** 257–266.

Moore, D. W., and P. G. Saffman, 1971: Structure of a line vortex in an imposed strain. *Aircraft Wake Turbulence and Its Detection,* J. H. Olsen, A. Goldburg, and M. Rogers, Eds., Plenum, 339–354.

Paull, R., and A. F. Pillow, 1985: Conically similar viscous flows. Part III. Characterization of axial causes in swirling flow and the one-parameter flow generated by a uniform half-line source of kinematic swirl angular momentum. *J. Fluid Mech.,* **155,** 359–379.

Pearson, C. E., 1965: Numerical solutions for the time-dependent viscous flow between two rotating coaxial disks. *J. Fluid Mech.,* **21,** 623–633.

Press, W. H., S. A. Teukolsky, W. T. Vetterling, and B. P. Flannery, 1992: *Numerical Recipes in FORTRAN: The Art of Scientific Computing.* 2d ed. Cambridge University Press, 963 pp.

Ray, P. S., B. C. Johnson, K. W. Johnson, J. S. Bradberry, J. J. Stephens, K. K. Wagner, R. B. Wilhelmson, and J. B. Klemp, 1981: The morphology of several tornadic storms on 20 May 1977. *J. Atmos. Sci.,* **38,** 1643–1663.

Rosenhead, L., Ed., 1963: *Laminar Boundary Layers.* Oxford University Press, 687 pp.

Rott, N., 1958: On the viscous core of a line vortex. *Z. Angew. Math. Phys.,* **9,** 543–552.

——, 1959: On the viscous core of a line vortex II. *Z. Angew. Math. Phys.,* **10,** 73–81.

Rotunno, R., and J. B. Klemp, 1985: On the rotation and propagation of simulated supercell thunderstorms. *J. Atmos. Sci.,* **42,** 271–292.

Saffman, P. G., 1992: *Vortex Dynamics.* Cambridge University Press, 311 pp.

Serrin, J., 1972: The swirling vortex. *Philos. Trans. Roy. Soc. London, Ser. A,* **271,** 325–360.

Shapiro, A., 1993: The use of an exact solution of the Navier–Stokes equations in a validation test of a three-dimensional non-hydrostatic numerical model. *Mon. Wea. Rev.,* **121,** 2420–2425.

——, 1996: Nonlinear shallow-water oscillations in a parabolic channel: Exact solutions and trajectory analyses. *J. Fluid Mech.,* **318,** 49–76.

Smith, R. K., and L. M. Leslie, 1978: Tornadogenesis. *Quart. J. Roy. Meteor. Soc.,* **104,** 189–199.

Stewartson, K., 1953: On the flow between two rotating coaxial disks. *Proc. Cambridge Philos. Soc.,* **49,** 333–341

Sullivan, R. D., 1959: A two-cell vortex solution of the Navier–Stokes equations. *J. Aeronaut. Sci.,* **26,** 767–768.

Thacker, W. C., 1981: Some exact solutions to the nonlinear shallow-water wave equations. *J. Fluid Mech.,* **107,** 499–508.

Trapp, R. J., and R. Davies-Jones, 1997: Tornadogenesis with and without a dynamic pipe effect. *J. Atmos. Sci.,* **54,** 113–133.

Tsonis, A. A., G. N. Triantafyllou, J. B. Elsner, J. J. Holdzkom II, and A. D. Kirwan Jr., 1994: An investigation of the ability of nonlinear methods to infer dynamics from observables. *Bull. Amer. Meteor. Soc.,* **75,** 1623–1633.

von Kármán, T., 1921: Über laminare und turbulente Reibung. *Z. Angew. Math. Mech.,* **1,** 233–252.

Watson, G. N., 1944: *A Treatise on the Theory of Bessel Functions.* 2d ed. Cambridge University Press, 804 pp.

Wurman, J., J. M. Straka, and E. N. Rasmussen, 1996: Fine-scale Doppler radar observations of tornadoes. *Science,* **272,** 1774–1777.

Yih, C.-S., F. Wu, A. K. Garg, and S. Leibovich, 1982: Conical vortices: A class of exact solutions of the Navier–Stokes equations. *Phys. Fluids,* **25,** 2147–2158.

Zandbergen, P. J., and D. Dijkstra, 1987: Von Kármán swirling flows. *Annu. Rev. Fluid Mech.,* **19,** 465–491.